UCRL-18463

cy. 2

University of California

Ernest O. Lawrence Radiation Laboratory

RECEIVED
LAWRENCE
RADIATION LABORATORY

NOV 22 1968

LIBRARY AND
DOCUMENTS SECTION

ON-LINE ISOTOPE SEPARATION AT THE HILAC

Joachim M. Nitschke

September 1968

TWO-WEEK LOAN COPY

This is a Library Circulating Copy which may be borrowed for two weeks. For a personal retention copy, call Tech. Info. Division, Ext. 5545

Berkeley, California

UCRL-18463 cy. 2

DISCLAIMER

This document was prepared as an account of work sponsored by the United States Government. While this document is believed to contain correct information, neither the United States Government nor any agency thereof, nor the Regents of the University of California, nor any of their employees, makes any warranty, express or implied, or assumes any legal responsibility for the accuracy, completeness, or usefulness of any information, apparatus, product, or process disclosed, or represents that its use would not infringe privately owned rights. Reference herein to any specific commercial product, process, or service by its trade name, trademark, manufacturer, or otherwise, does not necessarily constitute or imply its endorsement, recommendation, or favoring by the United States Government or any agency thereof, or the Regents of the University of California. The views and opinions of authors expressed herein do not necessarily state or reflect those of the United States Government or any agency thereof or the Regents of the University of California.

Submitted to Nuclear Instruments
and Methods

UCRL-18463
Preprint

UNIVERSITY OF CALIFORNIA

Lawrence Radiation Laboratory
Berkeley, California

AEC Contract No. W-7405-eng-48

ON-LINE ISOTOPE SEPARATION AT THE HILAC

Joachim M. Nitschke

September 1968

ON-LINE ISOTOPE SEPARATION AT THE HILAC*

Joachim M. Nitschke

Lawrence Radiation Laboratory
University of California
Berkeley, California

September 1968

Abstract

An on-line isotope separator was developed at the HILAC. The heavy ion beams impinges on a thin target, and the recoiling product nuclei are stopped in a solid or liquid catcher. They defuse out of this catcher at high temperatures and are ionized by a rotating electron cloud. The ions are focused with a rf quadrupole lens into a Paul mass filter. Thereafter they are subjected to analysis by conventional nuclear radiation spectroscopy. The principle of the instrument and the results of the first on-line runs are reported. A detailed report will be given elsewhere.

1. Introduction

This paper describes some of the results of an attempt to gain experience with an on-line isotope separator system at the heavy ion linear accelerator (HILAC). The project was initiated in 1966, and the first on-line runs for evaluating the performance of the complete system were made in July 1968.

The number of presently unknown beta unstable nuclei including neutron-, proton-, and alpha-emitters with half lives between 10^{-2} and 10^{2} seconds is estimated to be about 2,000[1]). Figure 1 shows a conventional nuclide chart with black squares representing stable nuclides and white squares the known radioactive isotopes[2]). The two lines designated $B_p=0$ and $B_n=0$ indicate the position of nuclides with zero binding energy for the last proton or neutron, respectively. It is evident from this chart that the number of unknown beta unstable nuclei exceeds the number of presently known. Knowledge about these white regions is most likely to increase our understanding of the nuclear structure.

Some nuclei will still have long enough half lives so that they can be studied by conventional techniques including wet chemistry. Identification of others will be possible by on-line techniques which do not include mass separation and which are capable of handling half lives as short as 1 ms. Most of the unknown nuclides, however, will require on-line techniques for unambiguous and direct identification.

Using Fermi's theory of beta decay, one can estimate that, excluding super allowed transissions, the shortest half lives of the unknown beta emitters will be about 10^{-2} seconds. This gives the first and very important parameter

for the construction of an on-line separator. Points of interest besides beta emission are alpha emission, delayed neutron- and proton emission, new double magic and deformed regions, Q-values and their implementation for the semi-empirical mass formula, nuclei of interest in astrophysics, and new trans-Lawrencium elements, in particular, in conjunction with the Omnitron.

After being convinced of the usefulness of on-line separation one has to decide on the method to be used, whereby the type of accelerator available is of primary importance. On-line systems at proton-synchrotrons, reactors, cyclotrons (also used as neutron generators), spontaneous fission sources, and heavy ion accelerators will differ mostly in target arrangements, fast chemistry, transportation and ion source while mass analysis, collection, alpha-, beta-, gamma-, and p-detection and data handling will be more uniform. Fig. 2 shows some possible ways of setting up an on-line separation system. The middle branch is the one most frequently used and also perhaps the most advanced (CERN, Orsay). Not included in Fig. 2 are some unique systems like the multi-dimensional fission study by Watson et al., in Berkeley, or laser time of flight systems.

Without discussing in detail the principles used in different on-line systems, a few problems and limitations should be pointed out, particularly in regard to fulfilling the most important requirement that the total transport time should be as short as possible.

1. Reactor fission studies are hampered by the alternative to either use the internal high neutron flux and cope with long (10 meter) transport lines, or use the external neutron beam which has orders of

magnitude lower intensities. The transport time in the first case would be in the order of several seconds unless the ionization takes place inside the reactor.

2. On-line systems using high energy protons face the basic problem of obtaining short diffusion times in targets of high effective thickness since the cross sections are small. In order to avoid the high radiation background produced by proton accelerators, most on-line projects include pump lines which again prohibit the study of very short lived isotopes.

3. The problem common to all projects is the lack of a universal ion source. Reaction products which are in gaseous form at or near room temperature can be used in conventional discharge-type ion sources (for example: Scandinavian type). Alkali, and with lower efficiency, group II elements have been used in surface ionization sources. Most other elements are easily lost by condensation on cold surfaces before they get into the ion source and/or are inefficiently ionized. It is not surprising, therefore, that the first elements studied on-line were alkalies and noble gasses.

4. A further problem which will require intensive study is the fast chemistry necessary to eliminate the ambiguity in Z. Little is known here. Most projects rely on physical means of separation like differences in surface ionization, catcher diffusion, evaporation rates and characteristic X rays in coincidence experiments. A heavy ion accelerator eliminates to a large extent the necessity for chemistry, since one can nearly always perform a differential experiment where the

bombarding ions differs by one proton.

5. At the HILAC a very promising approach had been taken a few years ago with the RAMA (Recoil Atoms Mass Analysis) project[3]). It corresponds to the top branch in the schematic diagram Fig. 2. Recoil atoms of a thin target are stopped in one atmosphere helium gas and can be collected with high efficiency (up to 80%) as demonstrated in many experiments. If one finds a way to get rid of the large amounts of helium without losing too much of the product nuclei, which then could be introduced in a discharge-type ion source, this seems to be a very promising method of on-line separation. It was also thought of directing the recoil carrying helium jet on a surface and removing the deposited activity with a sputtering ion source.

None of the very brief considerations given in this introduction points to a one-and-only method of on-line separation. Most of them are rather tailored to the specific experimental facilities. This is also the case with the fairly unique HILAC project.

2. General Description Of The On-Line Isotope Separator

The lower branch of Fig. 2 shows schematically the approach taken at the HILAC on-line separator project. Recoil target, recoil catcher and ionization have been combined into one unit to avoid losses and to gain speed. For more detailed discussion we refer to Fig. 3. The heavy ion beam impinges on a target, which is thin enough (about 1 mg/cm^2) to let product nuclei recoil into an ion source where they are caught in a solid or liquid catcher of high diffusivity. Electron bombardment keeps the ions source and the recoil catcher at a high temperature so that

short diffusion times can be achieved. After diffusing out of the catcher, the recoil nuclei are ionized by a rotating electron cloud and extracted into an electrostatic quadrupole which transfers and focuses the ions into the mass analyzer. As mass analyzer, we use a Paul mass filter[4]) which will later be described in detail. It is evident from Fig. 3 that neutral particles of undesired mass number have a chance to get through the whole separator as is the case in all straight-through machines. It is therefore necessary to separate neutral and ionized particles with a deflection system. In Fig. 3 the particles are deflected 90° onto an alpha counter which is meant to be an example for the radioactive counting equipment.

In addition to the neutral particles traveling down the instrument, an intense light is emitted from the ion source which in order not to be "seen" by the alpha detector has to be trapped in a light trap. The light trap also serves as a Faraday cup to read the ion current. To allow for offline tuning of the whole instrument, artificial recoils of thermal energy can be produced in a mass marker oven near the target (Fig. 3). This oven designed as a Knudsen cell produces a molecular beam consisting of ions of the same mass number as the radioactive isobar that is to be separated on-line. If the mass marker oven is charged with a natural element, it will in general produce several isotopic masses. This is a very welcomed feature because it allows adjustment of the resolution and transmission of the mass separator which are the two most important parameters. Except for the temperature of the ion source, all parameters of the separator can be adjusted with the mass marker before going on-line.

3. The Ion Source

The task of the ion source is threefold. It has to stop the recoils, defuse them out of the stopping material and ionize them.

The recoils produced in heavy ion reactions with HILAC ions of 10.38 MeV per nucleon can vary in energy from about 400 MeV to fractions of 1 MeV. Assuming no stopping in the target itself. The majority of all reactions for production of neutron deficient isotopes, however, involves recoil energies between about 5 and 20 MeV. Measurements of electronic stopping show that recoils of this energy can be stopped in .5 to 2 mg/cm^2 of material (independent of Z within a factor 2) [5]. 1 mg/cm^2 is, for instance, equal to 5×10^{-5} cm of tungsten or 5×10^{-4} cm of carbon.

The time τ it takes for a particle to defuse through a layer of material of thickness d depends on its diffusion coefficient D in this material and is given in first approximation by

$$\tau = \frac{d^2}{6D}$$

Therefore looking for a typical time constant τ of 10^{-2} sec the diffusion coefficient has to be

$$D = \frac{d^2}{6\tau} = \frac{25\text{x}10^{-10}}{6\text{x}10^{-2}} \approx 4\text{x}10^{-8} \ \frac{cm^2}{s} \text{ (for tungsten)}$$

and about $4\text{x}10^{-7}$ cm^2/sec in the case carbon is used as recoil catcher. Diffusion coefficients of this magnitude can be achieved only for very few elements at moderate temperatures (i.e., alkalies); most other elements require temperatures which in some cases approach the melting point of the base material. (Example: the diffusion coefficient of Li in 1,100°C Si is $1\text{x}10^{-5}$ cm^2/sec and for Bi at the same temperature $1\text{x}10^{-14}$

$cm^2/sec.$)

Since the diffusion coefficient is highly temperature-dependent

$$D = D_o e^{-\frac{E}{RT}}$$

a 10% increase in temperature typically results in one order of magnitude higher diffusion. Liquid metals have up to 10^5 * times higher diffusion coefficients and can be used as recoils catchers, but containment and high vapor pressures at the melting point create problems which have to be solved.

The following opposing conditions have to be met by a liquid catcher material:

1. Melting has to take place at a low vapor pressure ($< 10^{-5}$ torr) so that the ion source does not get saturated with vaporized and ionized catcher atoms, and so that the back of the water-cooled target and the insulators are not coated.

2. The metal has to have a high melting point so that the recoil atoms have a high vapor pressure in the liquid.

A look at the vapor pressure curves of all elements[6]) shows that only very few elements yield a reasonable compromise between both conditions. The following materials have been tried as recoil catchers: tantalum, tungsten, porous tungsten, graphite, graphite felt, liquid cerium and liquid zirconium.

The third task of the ion source, the ionization of the radioactive atoms, can be achieved in various ways, the most common being the gas

---

* The figures quotes in this paragraph on diffusion are only for illustration. They vary often many orders of magnitude.

discharge which has high ionization efficiency. The disadvantages of the discharge source for our application are:

1. A fairly long time delay results from the fact that the holdup time is equal to the discharge chamber volume divided by the "pumping speed" off the exit slit.

2. It requires high extraction voltages and yields therefore high energy ions which are incompatible with the quadrupole mass analyzer in its present form.

3. It produces a high background ion beam, which has to be kept at high energy to avoid beam blow-up.

For these reasons and in order not to duplicate work that is done, i.e., at CERN, it was decided to look into the possibility of electron bombardment ionization. Electron bombardment is in general about 10^4 times less efficient for ionization than a gas discharge. The ion current I_i depends on the electron density j_e, the cross section Q_e of the electron beam, the path lengths l_e of the electrons, the differential ionization cross section σ for electrons of a fixed energy, and the particle density ρ in the following form:

$$I_i = j_e Q_e l_e \sigma \rho$$

There are three free parameters to increase the ion current: j_e, Q_e and l_e. The cross section Q_e of the electron beam is limited by the size of the ionization chamber. We have therefore tried to increase the path length and the electron density.

For an understanding of the ion source it is useful to first

consider a simple magnetron as shown schematically in Fig. 4. It consists of an electron-emitting filament wire, a coaxial anode cylinder and two end plates in a magnetic field parallel to the common axis. At zero or weak magnetic fields, the electrons leave the wire to go radially to the anode which is at a positive potential U_a. With increasing magnetic field the electrons are bent into circular orbits, until at a certain critical field B_c the bending radius becomes smaller than the inner radius r of the anode cylinder, and the electron flow is cut off. This is illustrated in Fig. 4, where the electron current I_a is plotted versus the magnetic field H for different anode voltages. Anode voltage U_a^c at cut off and magnetic field B_c are related by Hull's[7]) equation:

$$U_a^c = \frac{e}{m} \frac{r^2 B_c^2}{8} .$$

A detailed description of the electron motion inside the magnetron is far from trival if space charge effects are taken into account. A theory developed by Brillouin[8]) describes the electrons as moving in a "solid cloud" around the cathode. The extremely high path length for the electrons makes this device attractive as an ion source.

The disadvantage in using the simple magnetron as an ion source is that an ion can be formed near the cathode as well as near the anode, so that the energy spread is nearly equivalent to the anode voltage times the charge of the ion. To avoid this, we have surrounded the cathode wire with a coaxial grid which is on anode potential and accelerates the electrons before they go on their circular orbits inside the anode cylinder. Thus, the anode region is field free and the extracted ions have only

minimal energies spread.

Figure 5 shows schematically hairpin-cathode, grid, and anode of the magnetron source. The ions, which have been formed, are extracted by a high transmission grid into the first, the so called transfer quadrupole. The second grid in Fig. 5 serves as electron mirror and is biased slightly above cathode potential to prevent electrons from ionizing the residual gas outside the ion chamber. The second improvement achieved by the introduction of the grid is that the electron density is much higher than in a simple magnetron because the space-charge limited electron flow in a coaxial diode is inversely proportional to the square of the anode-cathode distance. At very high electron currents though, a space-charge well is formed between grid and anode cylinder, which results in some spread of the ion energy. Fig. 6 is a photograph of four anodes of different materials after several on-line runs. Fig. 7 shows an anode chamber with accelerating grid and several catchers of different materials. The recoils enter through the grid covered hole.

To demonstrate the effectiveness of the electron cut-off, the mass-analyzed ion current of Mo-92 (the mass marker oven was filled with natural Mo) is plotted as a function of the magnetic field (Fig. 8). The peak ion current coincides with the cut-off field at 94 gauss indicating that it corresponds to the maximum electron path lengths.

4. Technical Details Of The Ion Source

As pointed out in the previous chapter the temperature of the recoil catcher has to be as high as possible to achieve short diffusion times. Since the recoil catcher is an integral part of the magnetron anode

chamber, it was decided to keep the whole at a high temperature. This has the advantage that the residence time of the gaseous recoil atoms on the chamber wall becomes extremely short. And for some elements we get a large contribution from surface ionization on the tungsten wall. The maximum temperature at which this type of ion source is expected to work is about 2,700°C. The vapor pressure of tungsten at this temperature is 4×10^{-5} torr, which at an ionization efficiency of 1 A/torr would yield 40 μA tungsten ion current. At this current the space-charge blowup would already reduce the transmission considerably. A further difficulty at even higher temperatures would be to maintain the structural stability of the chamber wall, and it would become a problem to control the temperature of the magnetron cathode. (At 2,727°C the electron emission of tungsten is 14 A/cm^2). It was therefore decided to set 2,700°C as the upper temperature limit. At this temperature the heat load on the target from the magnetron anode is about 80 watts, which is another factor preventing higher temperatures. Fig. 9 shows the ion source with the target and the extractor quadrupole.

The outer housing is milled out of one solid piece of OFHC copper and serves as a spool for the two Helmholtz coils, and supports all other parts of the source. Cooling lines traverse the whole copper block and are able to handle 5 kw heat load. The drawing Fig. 9 is in most parts self explanatory. The magnetron anode is surrounded by a filament for electron-bombardment heating. The total power available is about 4.5 kW giving an anode temperature of 2,700°C. The heating filaments are surrounded by only one heat shield, so that the target can be mounted close

to the ionizing region. Fig. 10 shows a plot of the heating power and the α-counting rate of a separated isotope versus anode temperature.

The ion source will accept recoils that leave the target under angles $\leq \pm 10^{\circ}$. The holes in the heat shield and in the magnetron anode, as well as the target anode distance, are chosen accordingly. The magnetron cathode is a hairpin filament made from 0.5 mm non-sag tungsten wire; the accelerating grid consists of 0.075 mm tungsten wire--20 wires per centimeter. The anode itself is made out of tungsten; we also have tried porous tungsten and (for lower temperatures) tantalum. It should be noticed that all insulators are "cold" and well hidden from metal vapors which could coat them. They do not have to be replaced. All insulators are boron nitride.

The Helmholtz coils, which provide a uniform magnetic field in the ionizing region, are vacuum impregnated with epoxy and encapsulated vacuum tight in an all-copper housing. There is no outgassing from the coils.

The vacuum system for the ion source consists of a liquid nitrogen-trapped 6" diffusion pump charged with DC 705. The vacuum chamber for the source is fabricated from stainless steel and has metal gaskets. Bake-out is possible but turned out to be unnecessary. The vacuum is in general 10^{-8} torr and during operation about 10^{-7} torr.

5. Operating Principle Of The Quadrupole Mass Filter

The transfer quadrupole is the next part of the separator which the ions encounter as they leave the ion source.

Since the transfer quadrupole is a special case of the more general mass-analyzing quadrupole, we will delay its discussion until a

later chapter.

The following serves as a brief explanation of how an electrostatic quadrupole field can be used for mass separation.

A three dimensional hyperbolic field is generally described as

$$\varphi = \varphi_o \, (\alpha x^2 + \beta y^2 + \gamma z^2);$$

because of $\Delta\varphi = o$ (Laplace equation)

it follows that $\alpha + \beta + \gamma = 0$.

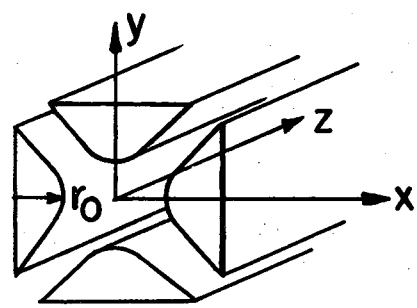

In our two-dimensional case, we have chosen

$$\gamma = 0$$

and $\alpha = -\beta = \dfrac{1}{r_o^2}$

so that the potential for $x, y = r_o$ is

$$\varphi = \varphi_o$$

The electrodes are connected to a dc and a rf potential, so that the potential inside the quadrupole is given by

$$\varphi = (U + V \cos \omega t) \, (x^2 - y^2) \, \frac{1}{r_o^2}$$

from this potential we get the electric field in x- and y-direction.

$$E_x = \frac{2}{r_o^2} \, (U + V \cos \omega t) x$$

$$E_y = - \frac{2}{r_o^2} \, (U + V \cos \omega t) y$$

And this leads immediately to the equations of motion

$$m\ddot{x} + \frac{2e}{r_o^2} \, (U + V \cos \omega t) \, x = 0$$

$$m\ddot{y} - \frac{2e}{r_o^2} \, (U + V \cos \omega t) \, y = 0$$

$$m\ddot{z} = 0$$

With the following transformations

$$\omega t = 2\xi, \qquad a = \frac{8eU}{mr_o^2\omega^2}, \qquad q = \frac{4\ eV}{mr_o^2\omega^2}$$

one can see that both equations can be regarded as a special case of Mathieu's equation which in its normal form reads

$$x'' + (a - 2q \cos 2\xi)\ x = 0$$

For q=0 we have the ordinary harmonic oscillator "a" being the spring constant. The cos term introduces a time dependence of this spring constant and it is obvious that if q is small compared to a, stable oscillations will result, otherwise the time dependent term will dominate and render an instable solution. One gets a more quantitative picture of these stability problems by looking at the stability diagram, which for low a and q values looks like this:

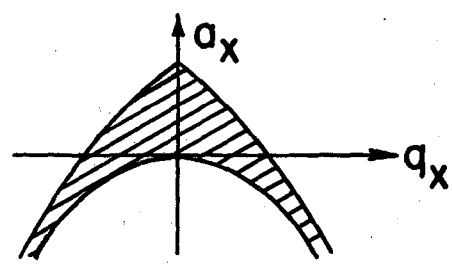

All a and q values in the shaded area give stable solutions for the Mathieu equation. For the x direction we have a direct correspondence between the normal Mathieu equation and the equation of motion. For the y direction we have to replace a by -a and we obtain the following stability diagram:

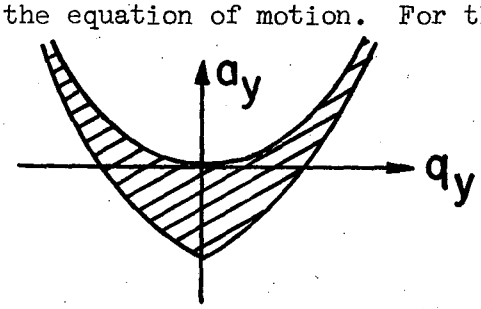

For the particle to go through the instrument it has to be stable in x and y so that the stability diagrams for the x- and y- motion have to be overlapped.

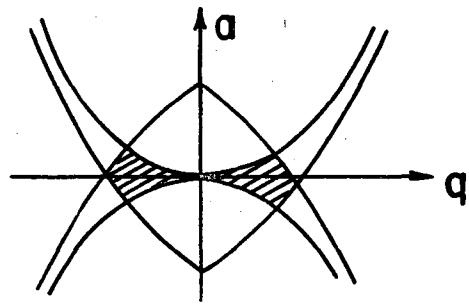

The shaded areas give a and q values for stable particle orbits in the quadrupole.

Referring back to the definition of a and q, and skipping constant factors (also frequency!), we have a~U/m and q~V/m; that is, a and q can be adjusted by changing the dc and rf voltage (at constant frequency ω).

In a practical instrument one operates always in the upper corner of the stability diagram and with a constant ratio U/V. This corresponds to a straight line in the stability diagram (Fig. 11). The U/V ratio is chosen so that only one mass number gives an a and q pair which is inside the stability region. By keeping the dc/rf ratio constant but varying their magnitude simultaneously, one can "push" different masses in the stability region and in this way use the instrument as a mass analyzer. Fig. 11 shows mass m_o inside the stability region; all other masses lie outside on the line called "mass scan line". The drawing is layed out so that if m_o were mass number 18, m_1 would be 19, m_2 equal to 20, m_{-1} equal to 17, m_{-2} equal to 16 etc. From Fig. 11 it is obvious that one can change the resolution by varying the dc/rf ratio. Lowering the dc/rd ratio means that the mass scan line intercepts a wider portion of the stability region and allows stable

orbits for more than one mass number.

After this brief explanation of the operating principle of the mass filter we can compare it with the more commonly used magnetic, electrostatic or time-of-flight analyzer. It is evident from the equations of motion that this instrument is a genuine e/m analyzer since neither the energy (like in the electrostatic analyzer) nor the momentum (like in the magnetic analyzer) enters. So even if an ion on a stable orbit collides with a rest gas molecule and is not too badly knocked out of its way it will continue through the instrument (we have operated at pressures of 10^{-4} torr). The input velocity of the ion is important only, in so far as, to allow for enough time inside the rf-dc field for undesired particles to get unstable. The greatest advantage besides the velocity independence is that the resolution can be adjusted from 0 (scan line on q axis) to infinite (scan line intercepting the corner of the stability region). This is not possible with most other mass separators. A further extremely valuable feature of the quadrupole is that its acceptance angle is about $\pm 15^{\circ}$ and the entrance aperture 6.5 mm, which again compares favorably with other instruments.

Since at the start of the whole project we did not have too clearly an idea what the on-line ion source would finally look like, the properties of the quadrupole seemed to be very attractive. Disadvantages are that it is a single-channel instrument, that it requires rather low energy ions, and that it is a straight-through machine. In the actual instrument cylindrical rods were used instead of hyperbolic ones (for cost reasons) Fig. 12. Their diameter was chosen as to minimize higher

order multipole components in the quadrupole field.

6. Computer Study Of The Quadrupole Mass Filter

Before the mass filter was combined with the magnetron ion source it was studied extensively as a separate unit. It was found that the theoretical relationships between a, q, U, V, e/m and the particle stability were perfectly fulfilled within the accuracy of the measurements (V could only be measured to 0.1%).

The parameter having the most influence on the resolution of the instrument was the ion velocity; this is theoretically well understood and became quite clear after the behavior of the unstable particles was studied with a computer. The size of the entrance aperture, which was thought to have a strong effect on the resolution, was found to be fairly uncritical.

To get a better understanding of the behavior of charged particles, in particular their amplitudes in a quadrupole field, a computer program for the CDC 6600 was developed to solve Mathieu's equation for different initial conditions. An on-line Cal Comp plotter draws the particle orbits in the x,z- and y,z- plane as well as a projection onto the x,y-plane and a perspective plot.

Figure 13 shows an example of the computer output. The mass of the injected particle is 28 AMU, its energy in z direction 85 eV, the energy components in x-and y-direction are plus and minus 0.5 eV, the input locations are -0.33, 0, +0.33 centimeters (which corresponds to an entrance aperture of 1/4"). With these three entrance locations and two velocity vectors for each location, 6 orbits are calculated in the

x,z and in the y,z plane. a and q were chosen so that double focusing in x and y results. This represents particles in stable orbits.

To show the influence of the rf phase angle at the time the particle is injected into the quadrupole field, Fig. 14 shows the orbits for 6 different phase angles 0, 1/3 π, 2/3 π, π, 4/3 π, 5/3 π, 2 π.* The particles enter at the center with x and y energy components of 0.01 eV. Beside the phase angle, the influence of the radial velocity on the amplitude is very obvious, if one compares Fig. 14 with Fig. 13. All other parameters are the same as in Fig. 13.

Without changing any of the parameters of Fig. 13, the mass of the injected particle was decreased from 28 to 27 AMU and the resulting particle orbits are plotted in Fig. 15. In Fig. 16 the mass was increased to 29 AMU, one AMU above the stable mass 28.

It is obvious that particles of mass 27 will not be transmitted through the quadrupole filter because the field-producing electrodes limit the maximum excursion to ±1.64 centimeter.

7. The Transfer Quadrupole

The connection between the ion source and the mass analyzer was originally accomplished by conventional ion optics consisting essentially of an einzel lens and a pair of deflecting electrodes. It turned out however, that this straightforward approach yielded a very low

---

* Because of the strong influence, the rf phase angle at the time of the injection of the particle has on its amplitude inside the quadrupole, we have tried to bunch the injected beam. This about doubled the transmission and improved the resolution.

transmission. A computer study of the extraction ion optic, for which Fig. 17 is an example, showed that the ion beam was hollow (which was expected because of the accelerating grid in the magnetron) and that the field between the electron mirror and the einzel lens acted strongly defocusing. Fig. 17 is a very simplified case where the ions are created in a plane perpendicular to the axis in the middle of the ion source. The computer program solves the particle orbit equation by taking the magnetic field off the Helmholtz coils, the electrostatic field of the electrodes, and the space charge created by the beam itself into account.

Several unsuccessful attempts to improve the transmission of the ion optical system lead to the decision to apply the strong focusing principle of a quadrupole lens. Instead of building an ordinary electrostatic quadrupole doublet or triplet in which the ion beam, loosely spoken, is first "squeezed" in x- and then y direction (z being the axial direction), we found that this can be done with one quadrupole, if it is connected to a rf source instead of dc. In this case the ion beam does not have to move from one quadrupole to the next in order to get squeezed in opposite directions, but the rf causes the quadrupole electrodes to change polarity fast enough to achieve the same effect in a single step. An analytical treatment of the motion of the ions in this quadrupole is very simple since it is a special case of the Paul mass filter with no dc voltage, corresponding to a=0 (Chapter 5). The equations of motion therefore are:

$$m\ddot{x} + \frac{2ex}{r_o^2} V \cos \omega t = 0$$

$$m\ddot{y} - \frac{2ey}{r_o^2} V \cos \omega t = 0$$

$$m\ddot{z} = 0$$

The orbits in the x,z and y,z plane are the same except for a phase factor. The computer program developed for the mass filter was used without any modifications.

The transfer quadrupole acts as a high pass filter for ions. Referring to the stability diagram Fig. 11, the case a=0 corresponds to the q axis being the mass scan line, and only particles with q values between 0 and 0.92 will have stable orbits. This corresponds for a given rf amplitude V, frequency ω and radius r_o to a mass range

$$\frac{4\ eV}{0.92\ r_o^2 \omega^2} \leq m \leq \infty$$

The higher the rf amplitude the higher the cutoff for low mass ions.* This is a very useful feature, because it allows to cut most of the background ions off, which are caused by the residual gas, and the catcher material (in the case of low Z catchers). The space charge burden on the beam is thereby greatly reduced.

It was found that when the rf was varied to attain optimum transmission of a certain mass, distinct maxima were encountered. Fig. 18 shows the ion currents through the mass filter for different ion energies as a function of the rf voltage. The fact that the first, second, and third maximum at 120 eV ion energy is occurring at the same rf amplitude

---

* Since quadrupole mass filters are used more and more "on-line" with gas chromatographs and sputtering experiments, this might be a good way of filtering out large amounts of He, Ar, etc.

as the second, fourth and sixth maximum at 60 eV ion energy, suggests the following explanation. The transmission maxima occur when a waist of the beam is located at the entrance aperture of the mass filter. The ratio of waist to average beam diameter becomes smaller with lower ion energies causing the small transmission variations shown in Fig. 18d. To support this explanation, the rf amplitudes for the four maxima in Fig. 18b, together with the necessary informations about mass number, energy, and geometry of the transfer quadrupole, were "fed" into the computer which calculated the particle orbits. The entrance aperture for the mass filter was located 17.5 centimeters from the starting point of the ion. The Fig. 19 shows that indeed a waist in x and y occurs at this location. Fig. 20 shows the particle orbits corresponding to the rf amplitude at the second maximum in Fig. 18b. Again a waist in the x,z and y,z plane occurs at about 17.5 centimeters. For the third and fourth maximum Fig. 21 and Fig. 22 are obtained. The waists are far less pronounced, and in Fig. 22 the particle is already unstable. This is also indicated by the sharp drop in the ion current in the middle of the fourth maximum of Fig. 18b. In praxis only the first or second maximum are used for operating the quadrupole.

With a slight modification in the rf power supply the transfer quadrupole can also be used for steering the ion beam; dc voltages of opposite polarity (contrary to the mass filter!) superimposed on the rf are fed to each pair of opposing electrodes, so that the beam can be deflected slightly. This is very helpful in directing the beam into the entrance aperture of the mass filter. Fig. 23 shows the magnetron anode,

extractor- and electron-mirror grid, and the transfer quadrupole.

8. Experimental Evaluation Of The Quadrupole Mass Filter

The quadrupole mass filter which was built for the on-line isotope separator has the following parameters:

rf frequency (constant): $\omega/2\pi = 1.000$ MHz

Geometric field parameter: $r_o = 1.6418$ cm

Radius of the quadrupole electrodes: $R = 1.8915$ cm

Ratio R/r_o for minimum higher order multipole components: $R/r_o = 1.152$

Length: $L = 57.5$ cm

Maximum ion energy for unit resolution: (Δm = 1AMU): $E_z^{max} = 105$ eV

Mass range: 0-300 AMU

Resolution: $m/\Delta m = 250$ (design value)

To test the resolution, 50 eV Xe ions were injected into the quadrupole. Figure 24 is a plot of the current at the Faraday cup versus mass number. The resolution is $m/\Delta m = 850$. The isotopic abundances are not reproduced correctly because of slight inaccuracy in the tracking of the rf and dc voltages. This effect disappears at lower resolution and is of little importance in an isotope separator.

Most tests concerning the performance of the quadrupole as a mass spectrometer were made with a 20 stage photo multiplier, counting the transmitted ions and storing the number of counts in a multi-channel analyzer which was operated in the multi-scaler mode. The stepping off the MCA was synchronized with the mass scan. Fig. 25 shows a typical spectrum obtained by pulse counting. It should be noted that even at low resolution the interference of adjacent peaks can be made small. Futher-

more the logarithmic display in Fig. 25 is a good demonstration of the peak asymmetry which is a basic artifact of all quadrupole- and monopole-mass filters. To understand this we have to refer back to the stability diagram Fig. 11. It should be remembered that on the mass scan line $m_1 > m_0 > m_{-1}$. If one wants to bring a larger mass, say m_1, into the "stability corner", one has to increase the rf and dc voltages U, V. Mass m_1 then enters the stable region under a very flat angle so that noise on the rf and dc produces a large "noise" in mass number; which results in the flat slope of the mass peaks on the side of the lower mass (in this case m_0). If one increases the rf and dc voltages further, mass m_1 leaves the stability region nearly perpendicular to the stability boundary where rf and dc instabilities have little influence on the mass number; which thus results in a steep slope of the mass peak on the side of the higher mass (m_2). The stability of U and V is 3×10^{-4}; the stability of the frequency is 1×10^{-6}. The angle of entrance into the stability diagram would not have any influence on the slope of the mass peaks if the rf and dc voltage as well as the frequency were absolutely stable.

9. Performance Of The Complete Separator And On-Line Runs

Several tests of the complete separator were made before it was installed at the accelerator. In particular one would like to determine the over-all efficiency. In other words, what is the chance of a recoil atom leaving the target, to get into the ion source, to defuse out of the catcher before it decays, and to become ionized, to be transfered into the mass filter, to get through the mass filter and to be

deflected onto the detector? Only very few of these variables can be theoretically deduced with any degree of confidence, and they will vary widely; whereby the following parameters are linked together:

1. The type of nuclear reaction will influence the recoil energy and consequently the penetration depth into the catcher and the diffusion time.

2. The type of nuclear reaction and the target thickness will influence the absorbtion in the target and the angular spread of the recoils.

3. The kind of element that is produced in the nuclear reaction will influence the diffusion out of the catcher and the probability of electron bombardment-and surface ionization.

4. The transmission that can be achieved through the quadrupole mass analyzer depends on the mass number of the isotope to be studied.

Preliminary results concerning these four points are:

1. Sm bombarded with 166 MeV O16 produces among other nuclei Yb 154 with a half life of 0.39 seconds[9]). The recoil energy is 15 MeV. By comparing the yield for Yb 154 with the yield for longer lived isotopes made during the same bombardment and taking into account the reduced cross section, it was found that no holdup due to slow diffusion in the catcher can be observed at this half life.

2. From measurements of the angular spread of recoils by Donovan et al.,[10]), it can be estimated that with the present geometry about 50% of the recoils enter the ionization chamber.

3. The sensitivity of the magnetron ion source is easily established for gasses. Using common gasses like N_2, O_2, CO_2, He, Ne, Ar, Kr, and Xe it was found that the sensitivity varies between 2 A/torr and 20 A/torr.

It has to be realized, however, that the pressure inside the ionization region is not known precisely. We therefore used another independent method to establish the sensitivity.

A small piece of Mo wire was put in the ionization chamber and the temperature raised to 1981° K. The resolution of the mass filter was adjusted so that all Mo isotopes were transmitted. This resulted in an ion current of 50nA. The vapor pressure of Mo at 1981° K is 1.4×10^{-7} torr[11]). If one assumes a loss of about 80% at the entrance aperture of the quadrupole, the extractor grid, and in the transfer quadrupole, the sensitivity of the ion source is about 1.5 A/torr. This experiment was repeated at different temperatures. A sensitivity of 2 A/torr is equal to an ionization efficiency of about 1%. The weak point of this method is that an error in the temperature measurement results in a large error in the vapor pressure and consequently in the sensitivity.

Therefore a third determination of the ionization efficiency was done with Am 241. A known amount of activity was placed on a small platinum disc, which then was spot welded onto the inner wall of the ionization chamber; moderate heating released the Americium. The ionized portion of the activity which was extracted out of the ion source was collected on a plate and counted. After a correction for the neutral particles

that might have reached the collector the ratio of the activities gave an ionization efficiency of 3.5%.

All measurements were taken with the following operating parameters of the ion source:

Magnetron anode voltage: $U_a = 250$ V

Electron current measured at the cathode: $I_a = 500$ mA

Extractor voltage: $U_{ex} = 35$ V

Electron mirror voltage: $U_{mirr} = 300$ V

Ion energy: $U_{ion} = 80$ V

Magnetic field: H = 100 Gs (approx.)

Figure 26 shows schematically-typical potentials at different parts of the separator. (The current values indicate the upper limits of the power supplies.)

4. In the present quadrupole analyzer the transmission has to be reduced to about 1% to obtain less than 1% interference from adjacent peaks at mass number 150. This is demonstrated in an experiment where Sm 152 was separated from natural Samarium (off line).

The mass marker oven (see Fig. 5) was charged with natural Samarium and heated so that the ion current at the Sm 152 peak was about 20 nA. The adjustment of the proper resolution necessary to separate Sm 152 was done by observing the spectrum Fig. 27. The ion current onto the Faraday cup was amplified, fed into a current-to-frequency converter, "stored" in a multi-channel analyzer, and transferred onto a tape. The plotting of the spectrum was done by a computer. After stopping the scanning of the spectrum and adjusting the mass filter for mass 152, a current of 10 nA

Sm 152 was deflected onto a 1" platinum collector which was located at the position of the alpha detector in Fig. 3. 53 ng Sm 152 was collected. The sample was submitted to our mass spectrometer group which analyzed it with a magnetic mass spectrometer. The result is shown in Fig. 28*. The separation factors† are 224 for Sm 154, 820 for Sm 149, and 860 for Sm 147. The other isotopes cannot be used to calculate separation factors because of possible interference from other rare earths. These separation factors can be considered satisfactory for most on-line work. They might have been even better, considering that there was an accident during the separation which involved natural Samarium atoms.

In conclusion the following very preliminary estimate of the overall transmission of the on-line separator can be made.

1. Transfer of the recoils into the ionizing chamber: $\eta_1 = 5\text{x}10^{-1}$
2. Ionization efficiency: $\eta_2 = 1\text{x}10^{-2}$
3. Extraction from ion source, transfer, and collimation: $\eta_3 = 2\text{x}10^{-1}$
4. Transmission of the mass filter (at mass 150): $\eta_4 = 10^{-2}$

Total transmission: $\eta = \eta_1\eta_2\eta_3\eta_4 = 1\text{x}10^{-5}$

This figure has to be compared with the actual figure deduced from on-line runs.

For the first on-line runs we chose the reactions Sm(Cl2,xn)Er, Sm(Nl4, sn) Tm, and Sm(Ol6,xn) Yb. With full energy beams (10.38 MeV/nucleon)

---

* Thanks to Maynard Michel who performed the analysis.

† The separation factor is defined as the ratio of the natural abundance of an isotope versus the abundance after separation; both ratios taken with respect to the isotope to be separated.

and x equal to 6,7,8, or 9, alpha-emitting isotopes of the rare earth are produced. They require only a simple surface barrier detector for unambiguous identification by their α-decay energy and half life, and have high enough mass numbers to prove the usefulness of the mass filter.

Figure 29 shows the result of the separation of Er 152 which has a half life of 10.7 seconds. The lower part of Fig. 29 is the alpha spectrum of the reaction Sm 147 (C12,xn) taken with a wide transmission range of 150 ± 10 AMU. In the upper portion the mass filter was tuned for mass 152 and unit resolution. Ho 152 and Er 152 are now the major peaks. There is a slight interference from Er 153. The counting rate for Er 152 is about 2 counts/minute.

Assuming a cross section of 10 mb for the reaction Sm 147 (C12, 7n) Er 152, a carbon 12 beam of 2 μA, and a target with 1 mg/cm^2 Sm 147, the formation rate for Er 152 is 4×10^5 particles/minute. This corresponds to a total transmission of 0.5×10^{-5}, and compares favorably with the calculated transmission, if one considers a certain amount of absorption in the target itself.

Figures 30, 31, and 32 show the complete ion source, the target with the mass marker oven, and a microphotograph of the graphite felt used for stopping the recoils.

10. Summary And Conclusions

It has been shown in this paper, that the unusual combination of recoil target, efficient electron bombardment source and a Paul mass filter can be used as an on-line isotope separator. Diffusion times in hot solid catchers are short enough to study sub-second isotopes.

Without altering the principles, by mere changes in geometry a factor 100 could be gained in over all transmission. These changes would include all main parts of the separator, ion source, transfer quadrupole, and mass filters.

11. Acknowledgements

I wish to express my appreciation to Dr. Albert Ghiorso for his continued interest in this work and the inspiring and stimulating atomsphere he and his group have provided.

Only a small fraction of what was accomplished would have been possible without the ingenuity of C. A. Corum and his unconventional, efficient approach to mechanical designing. I am very grateful for his help.

I wish to thank R. Grazier for the design of the rf power supply for the quadrupole.

The splendid cooperation of the accelerator technicians and the HILAC crew is greatly appreciated.

The author was the recipient of a German Academic Exchange Service (DAAD) fellowship during part of the research.

12. Figure Captions

1. Chart of nuclides. Black squares representing stable isotopes, open squares known radioactive isotopes. Lines $B_p=0$ and $B_n=0$ show the position of nuclei with zero binding energy for the last proton or neutron respectively.
2. Possible ways of on-line isotope separation.
3. The HILAC on-line isotope separator.
4. Anode current of a simple magnetron as a function of the magnetic field, for different anode voltages.
5. The magnetron ion source (schematic).
6. Magnetron anodes after several on-line runs. (left to right, top row) 0.25 mm tungsten, porous tunsten, (bottom row) tantalum, 0.13 mm tungsten.
7. Magnetron anode with accelerating grid and catcher. Different catcher materials in front. (left to right) graphite felt, graphite, porous tungsten.
8. Ion current after mass separation as a function of the magnetic field in the magnetron source.
9. Cut-away view of the magnetron source.
10. Alpha counting rate at the alpha detector (see Fig. 3), and heating power as a function of the temperature of the magnetron anode. (Catcher: graphite felt).
11. Stability diagram for the quadrupole mass filter.
12. The rod structure for the quadrupole mass filter. (Total length between insulators 50.80 cm).

13. Computed stable orbits for 6 particles in the quadrupole filter. Top: projection of the orbits on the x,y-plane, Middle: x-component of the particle orbit, Bottom: y-component. Particles differ in input vector. Mass: 28 AMU.
14. Five particles injected into the quadrupole at different rf phase angles. Mass 28 AMU.
15. Example for instable particle orbits. All parameters the same as Fig. 13, except Mass: 27 AMU.
16. Same parameters as Fig. 13 but Mass: 29 AMU.
17. Computed particle orbits in the extraction region of the magnetron source. Extractor potential: 50 V, electron mirror: 50 V, Helmholtz field: 100 Gs. Dotted lines are equipotential lines.

18,(a),(b),(c),(d). Ion current through the transfer quadrupole as a function of the rf voltage on the quadrupole electrodes, for different ion energies.

19. Particle orbits through the transfer quadrupole at a rf voltage corresponding to the first maximum in Fig. 18b.
20. Same as Fig. 19 except rf voltage is higher (2nd maximum in Fig. 18b).
21. Same as Fig. 19 except rf voltage is higher (3rd maximum in Fig. 18b).
22. Same as Fig. 19 except rf voltage is higher as in all previous cases (4th maximum in Fig. 18b). Particle is in a instable orbit.
24. High resolution mass spectrum of Xe. Ion current measured with a faraday cup.
25. Low resolution Xe-spectrum. Ion pulse counting with 20 stage multiplier and MCA storage.

26. Electrical potentials at different parts of the on-line separator. (Arrows with circles indicate variable and r e g u l a t e d power supplies.
27. Mass spectrum of natural Sm as used for separating Sm-152 (refer to Chapter 9).
28. Mass spectrum of separated Sm-152 sample, as analyzed with a magnetic mass spectrometer.
29. Alpha spectrum of $Sm(C^{12},xn)$ bombardment (bottom). Same spectrum after turning on mass filter for separating mass 152 (top).
30. Exploded view of the magnetron ion source. (With "old" ion optics!).
31. Target holder. Left: beam side. Right: ion source side with heat shield and mass marker oven.
32. Micro photography of graphite felt catcher.

13. References

*This work was done under the auspices of the U. S. Atomic Energy Commission.

1. I. Bergström, Nucl. Instr. and Meth. 43, 116 (1966).

2. G. Rudstam, Nucl. Instr. and Meth. 38, 282, (1965).

3. A. Ghiorso, private communication.

4. W. Paul, M. Raether, Zeitschrift f. Physik 140, 262 (1955).

5. J. M. Alexander, L. Winsberg, UCRL-8997 (1960).

6. R. E. Honig, RCA Review Vol. XXIII, 4, 567 (1962).

7. A. W. Hull, Phys. Rev. 18, 31 (1921).

8. L. Brillouin, Proc. IRE 32, 216 (1944).

9. R. D. MacFarlane, Phys. Rev. 136, B941 (1964).

10. P. F. Donovan, B. G. Harvey, W. H. Wade, UCRL-9060 (1964).

11. See 6.

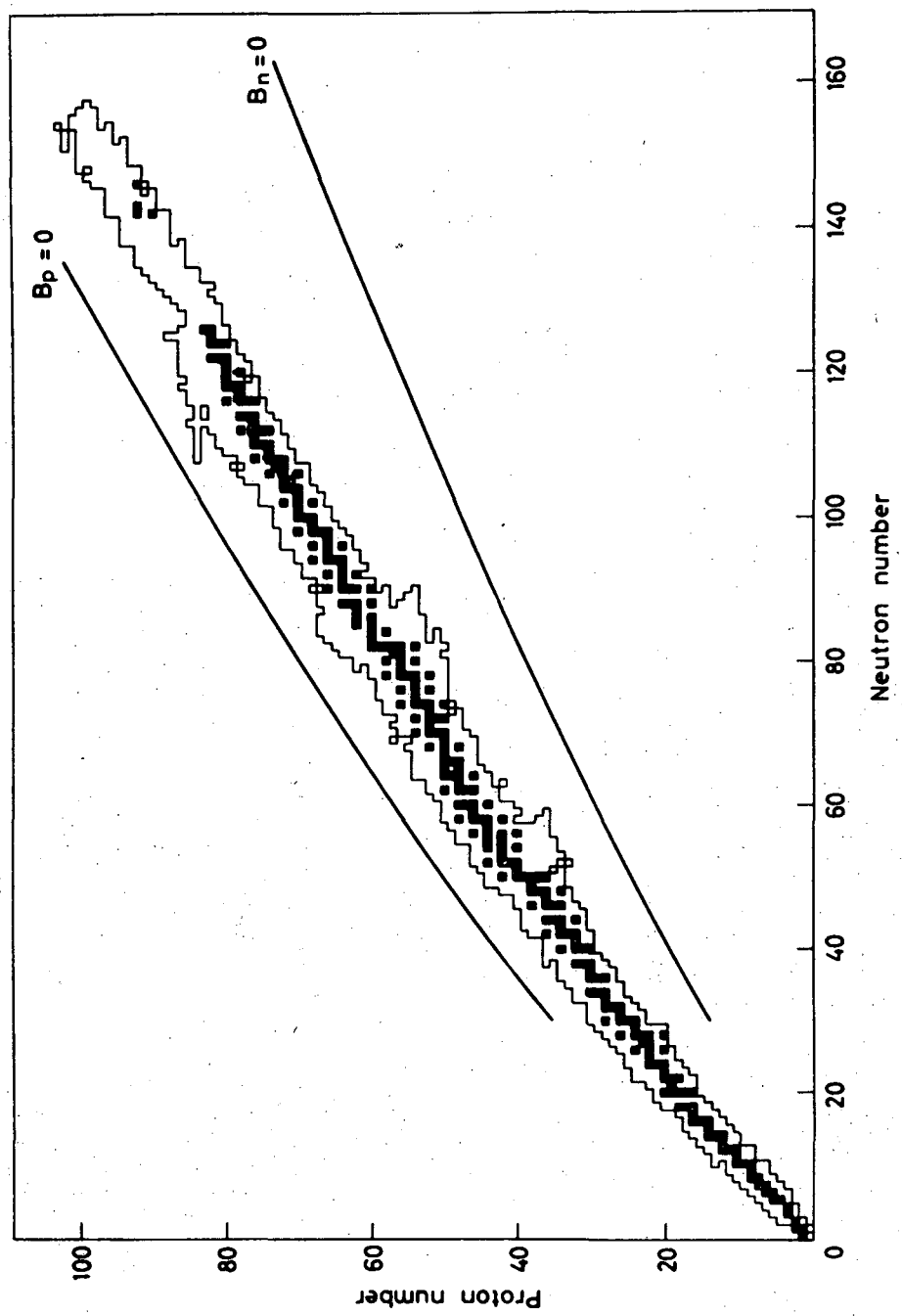

XBL 688-5749

Fig. 1

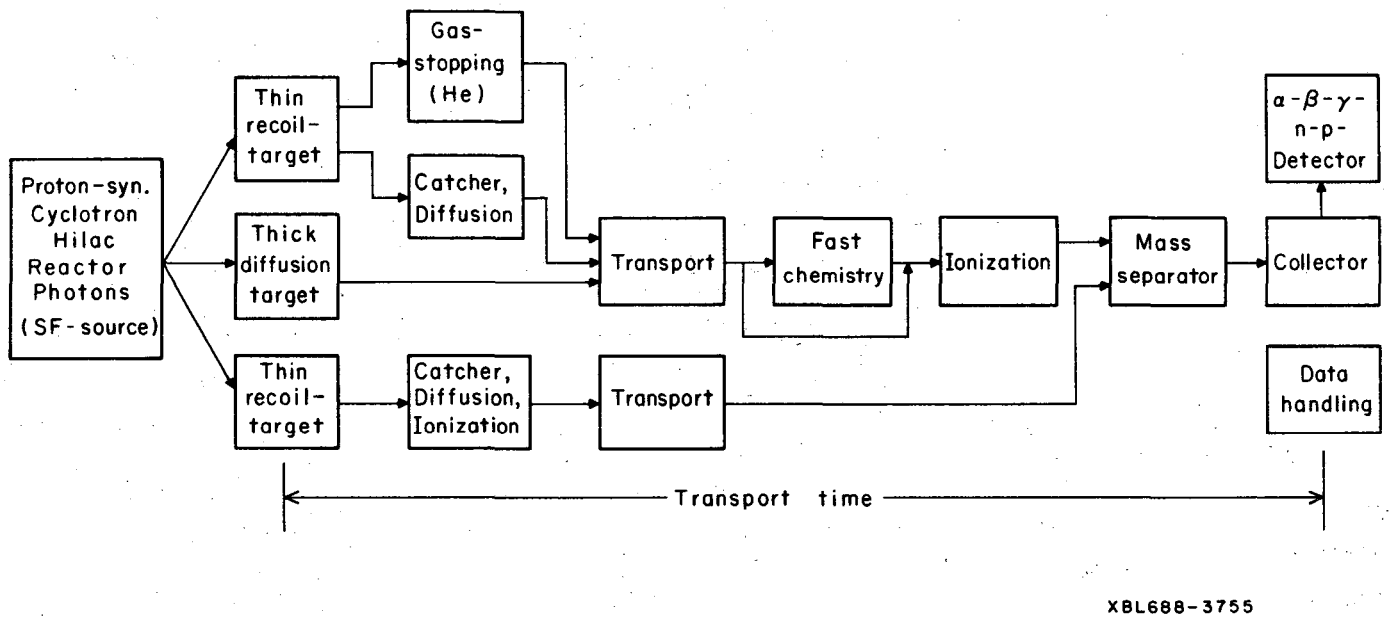
Proton-syn.
Cyclotron
Hilac
Reactor
Photons
(SF-source)
Thin recoil-target
Thick diffusion target
Thin recoil-target
Gas-stopping (He)
Catcher, Diffusion
Catcher, Diffusion, Ionization
Transport
Transport
Fast chemistry
Ionization
Mass separator
Collector
α-β-γ-n-p-Detector
Data handling
Transport time
XBL688-3755

Fig. 2

ON LINE ISOTOPE SEPARATOR

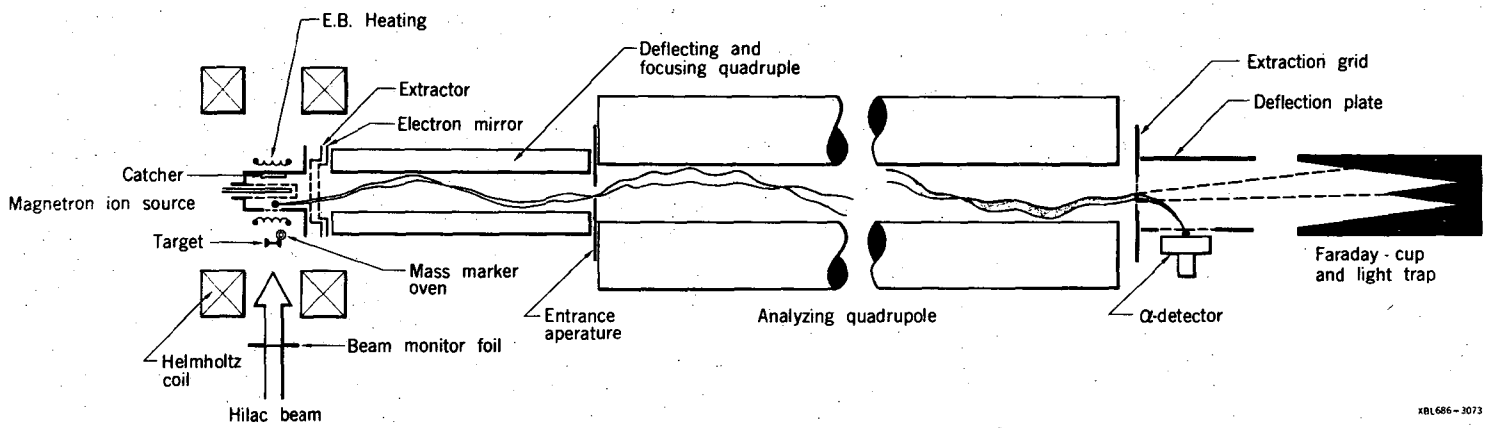

Fig. 3

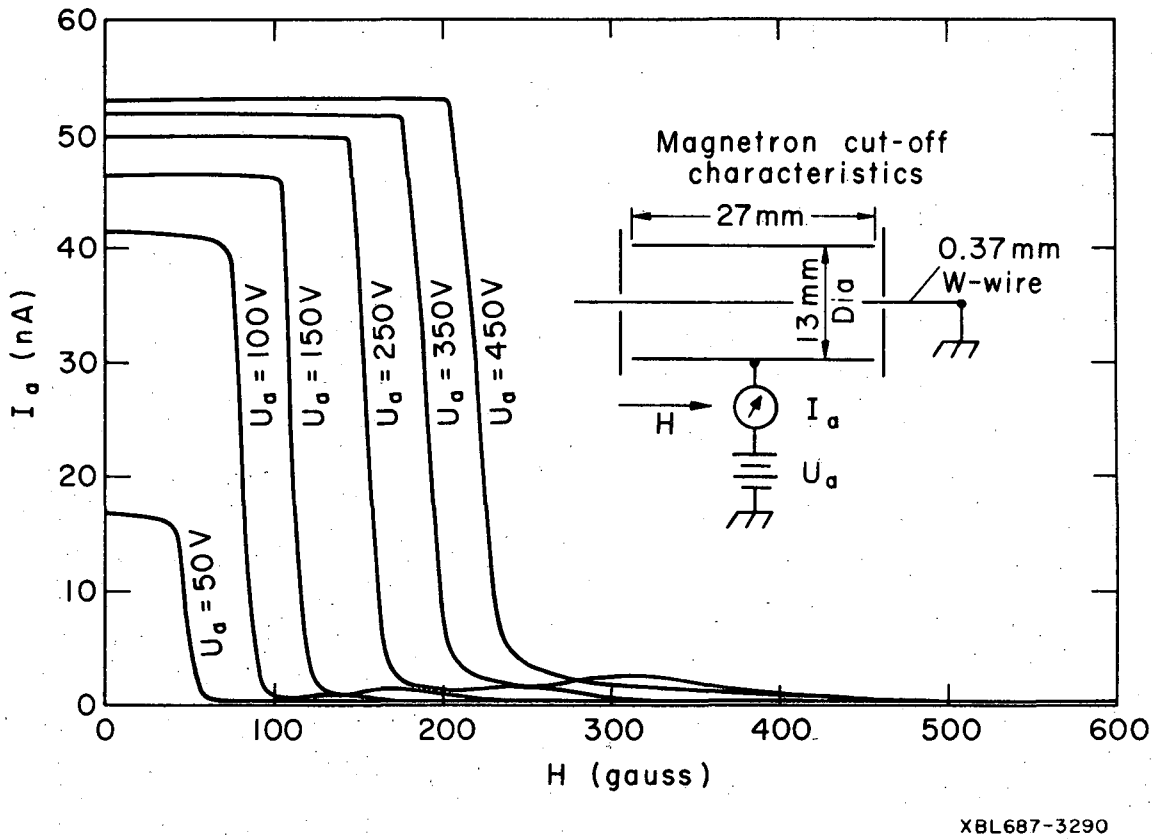
Magnetron cut-off characteristics
27mm
0.37mm W-wire
13mm Dia
H
I_a
U_a
U_a = 50V
U_a = 100V
U_a = 150V
U_a = 250V
U_a = 350V
U_a = 450V
I_a (nA)
H (gauss)
0
10
20
30
40
50
60
100
200
300
400
500
600
XBL687-3290

Fig. 4

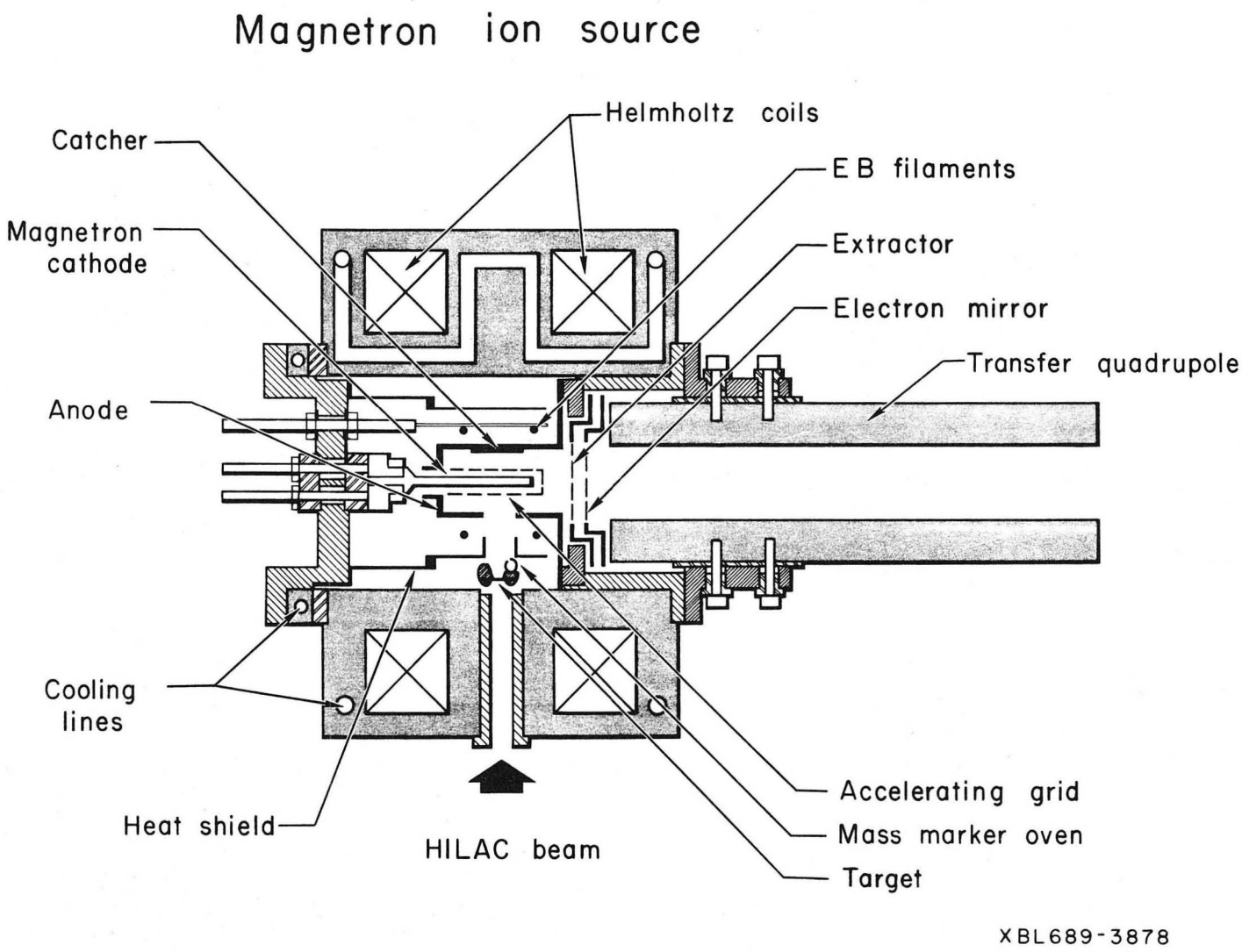
Magnetron ion source
Helmholtz coils
Catcher
E B filaments
Magnetron cathode
Extractor
Electron mirror
Transfer quadrupole
Anode
Cooling lines
Heat shield
HILAC beam
Accelerating grid
Mass marker oven
Target
XBL689-3878

Fig. 5

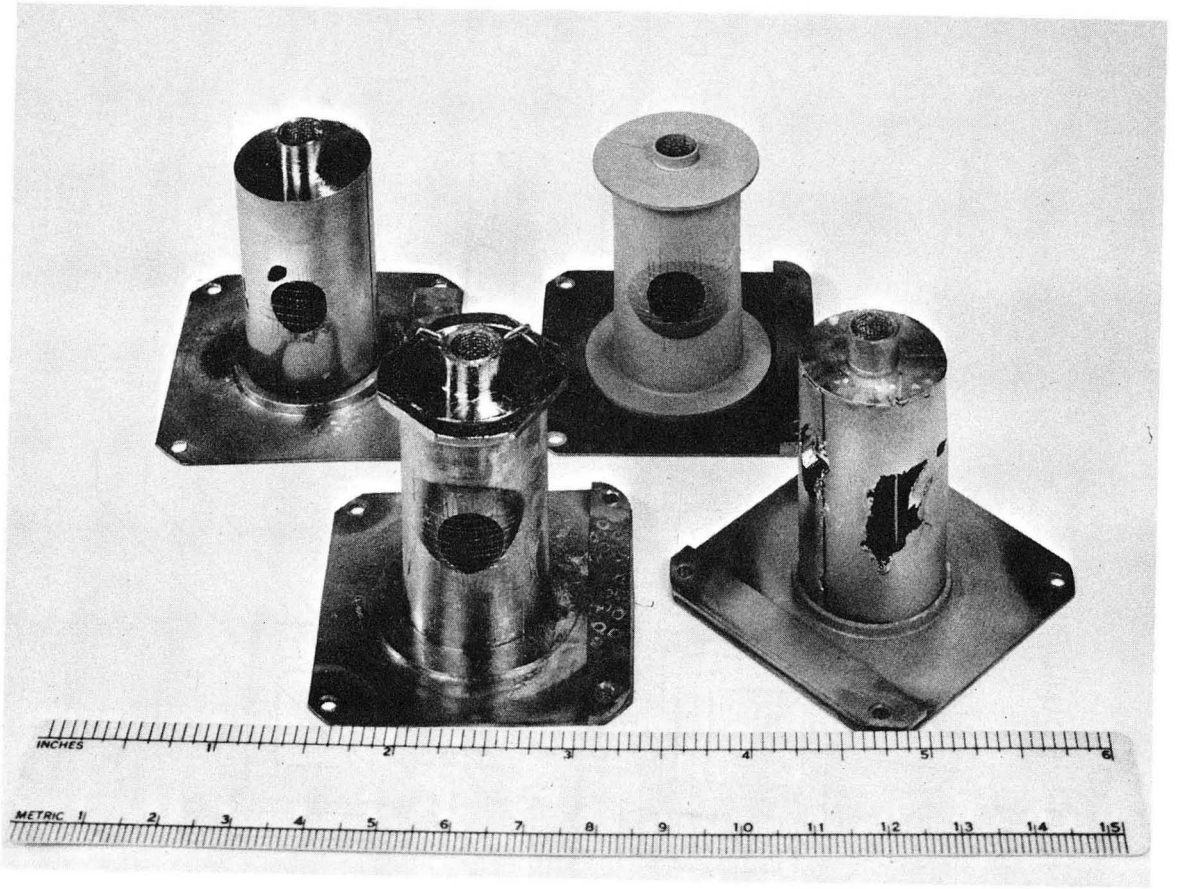

CBB 688-4884

Fig. 6.

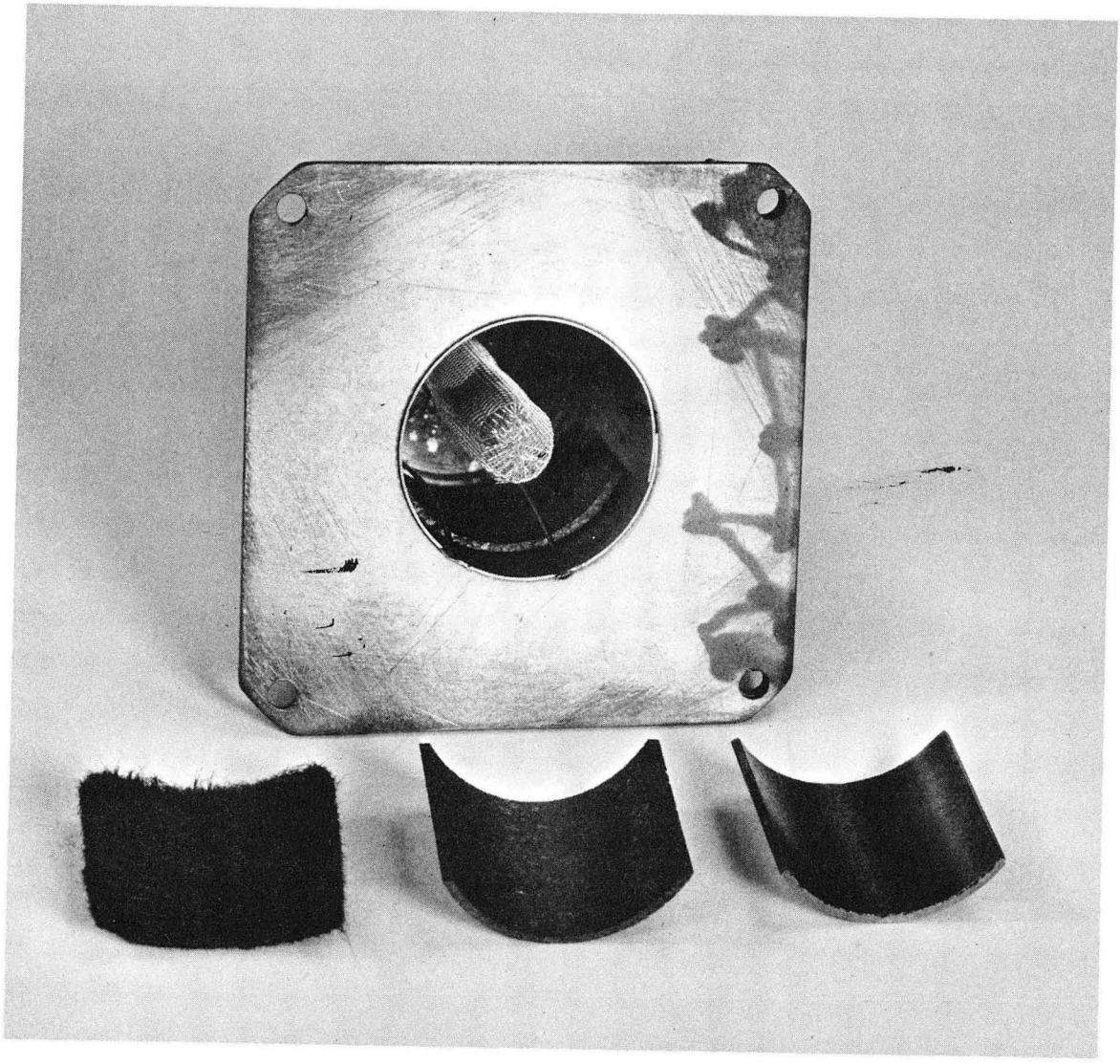

CBB 688-4886

Fig. 7.

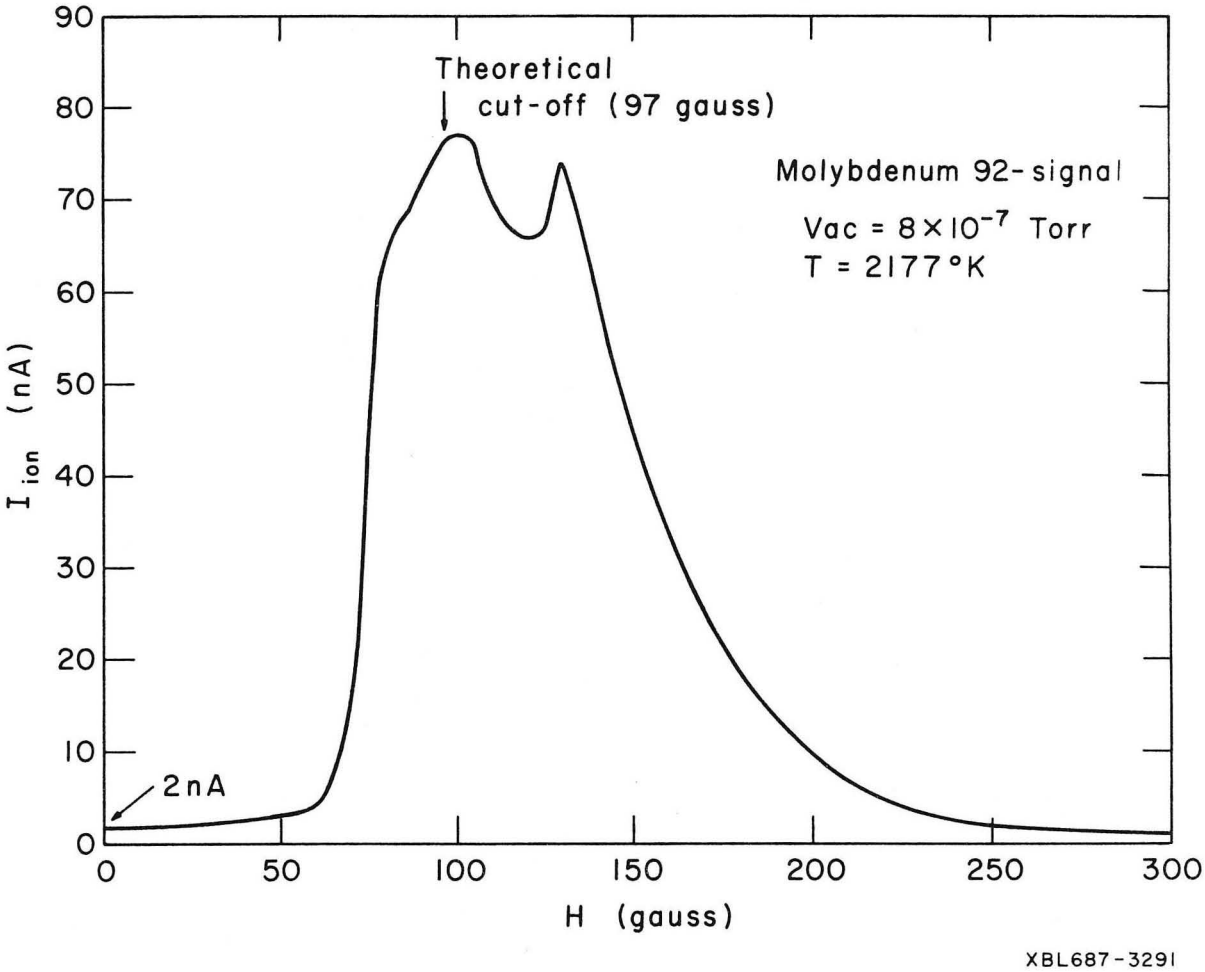
Theoretical
cut-off (97 gauss)
Molybdenum 92-signal
Vac = 8×10⁻⁷ Torr
T = 2177°K
2nA
I ion (nA)
H (gauss)
0
10
20
30
40
50
60
70
80
90
0
50
100
150
200
250
300
XBL687-3291

Fig. 8

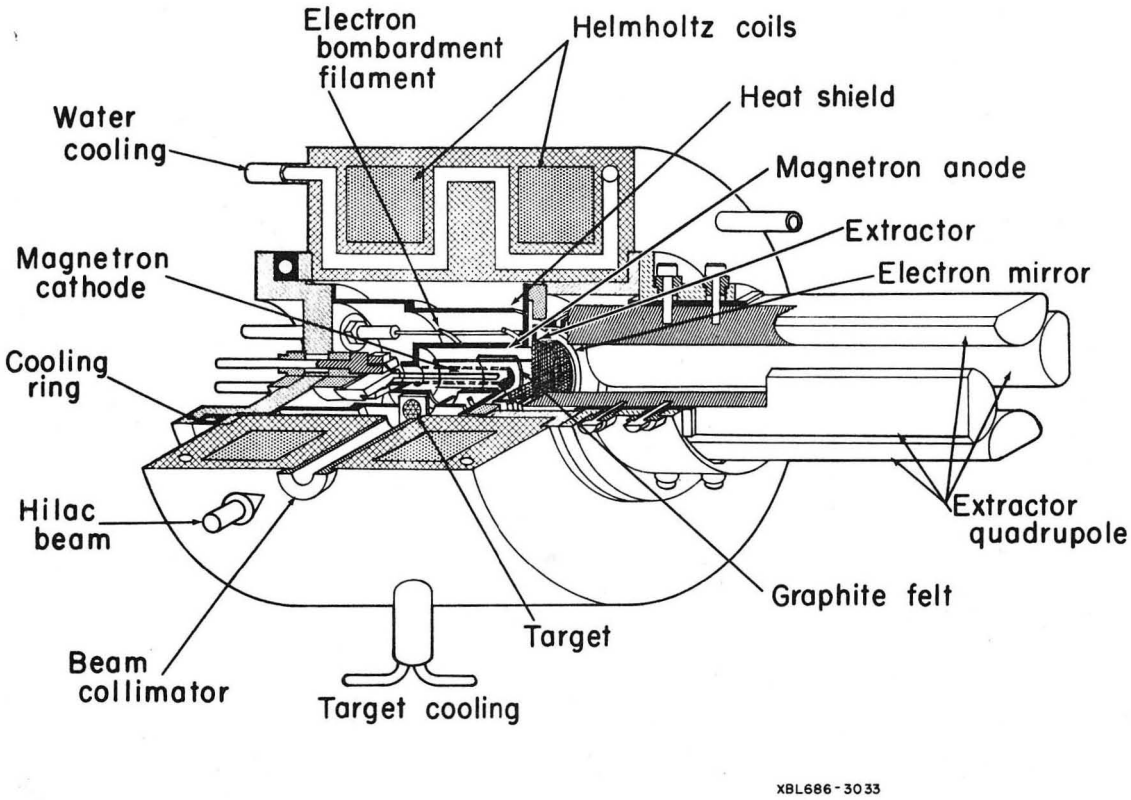
Electron bombardment filament
Helmholtz coils
Heat shield
Water cooling
Magnetron anode
Extractor
Magnetron cathode
Electron mirror
Cooling ring
Hilac beam
Extractor quadrupole
Graphite felt
Target
Beam collimator
Target cooling
XBL686-3033

Fig. 9

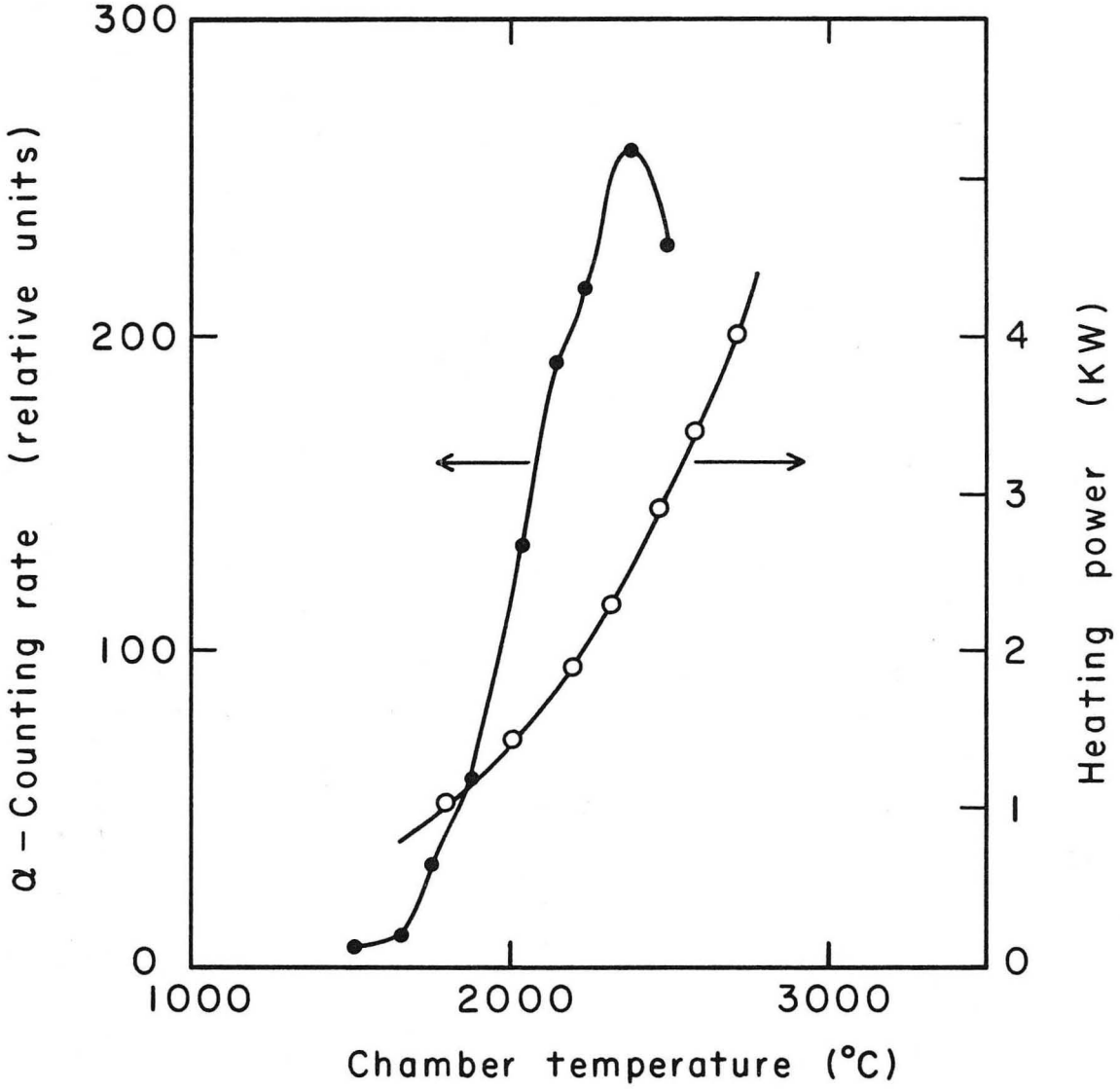

XBL688-3754

Fig. 10

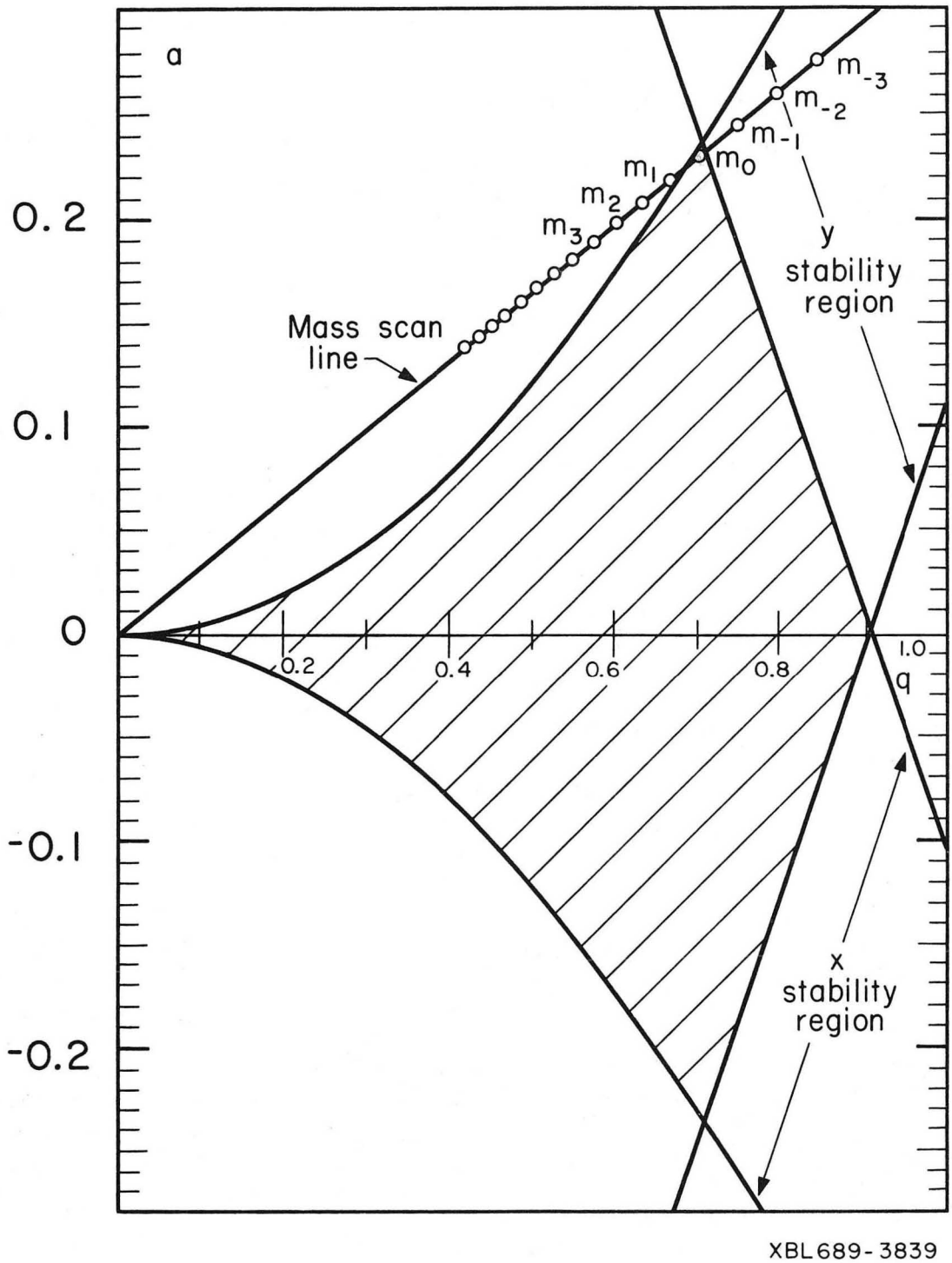
a
0.2
0.1
0
-0.1
-0.2
0.2
0.4
0.6
0.8
1.0
q
Mass scan line
m_3
m_2
m_1
m_0
m_{-1}
m_{-2}
m_{-3}
y stability region
x stability region
XBL689-3839

Fig. 11

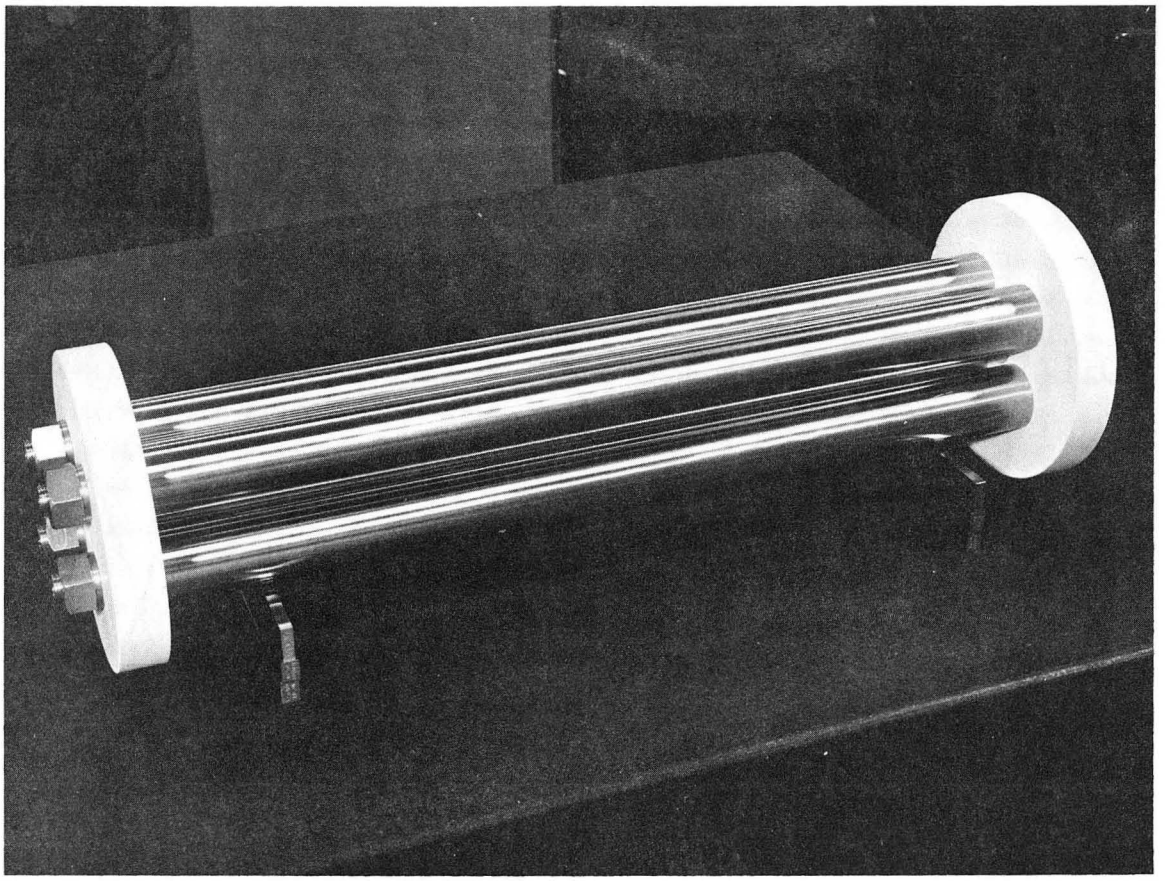

HIA 1470

Fig. 12.

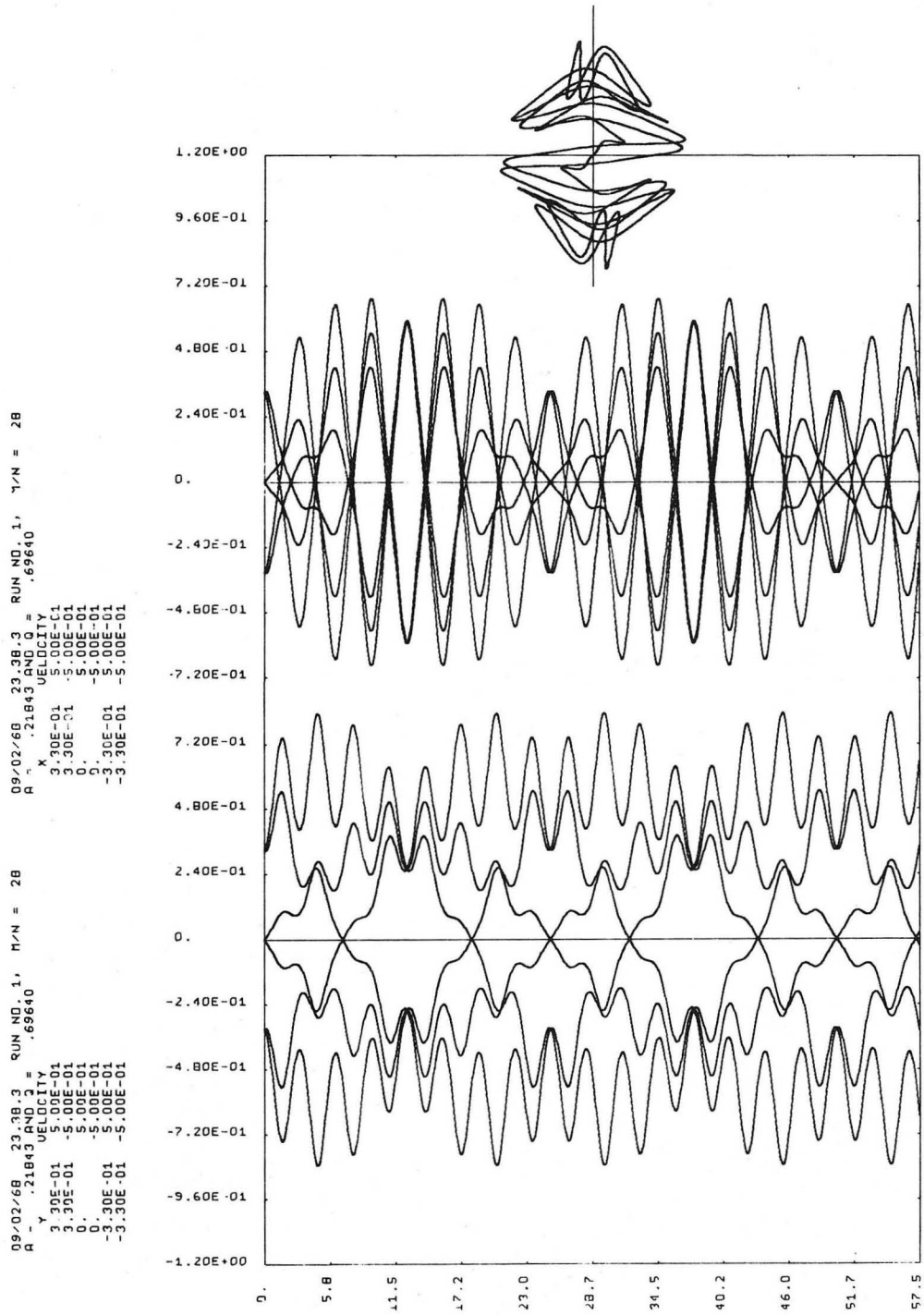

XBL 689-5817

Fig. 13

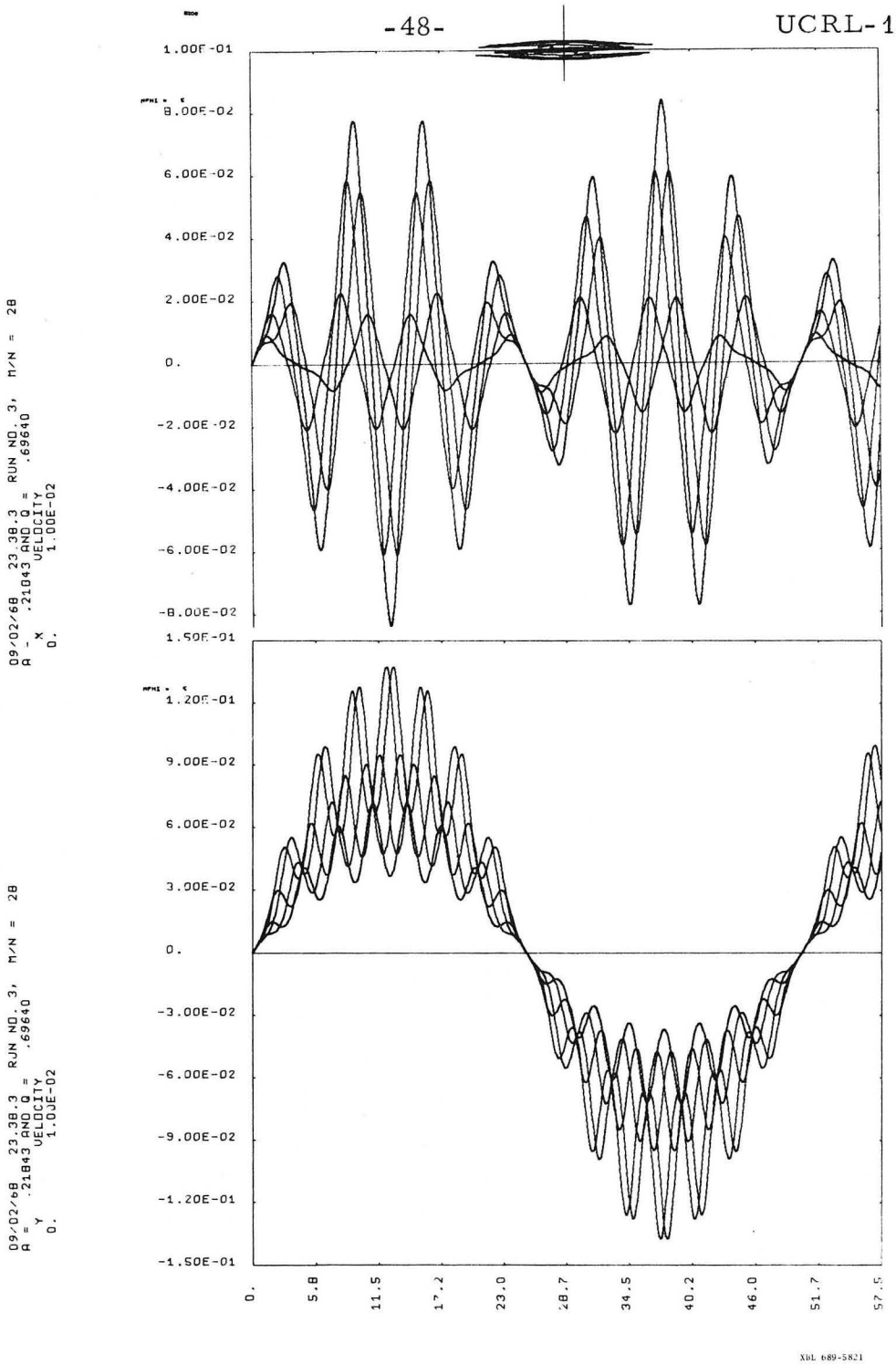

XBL 689-5821

Fig. 14

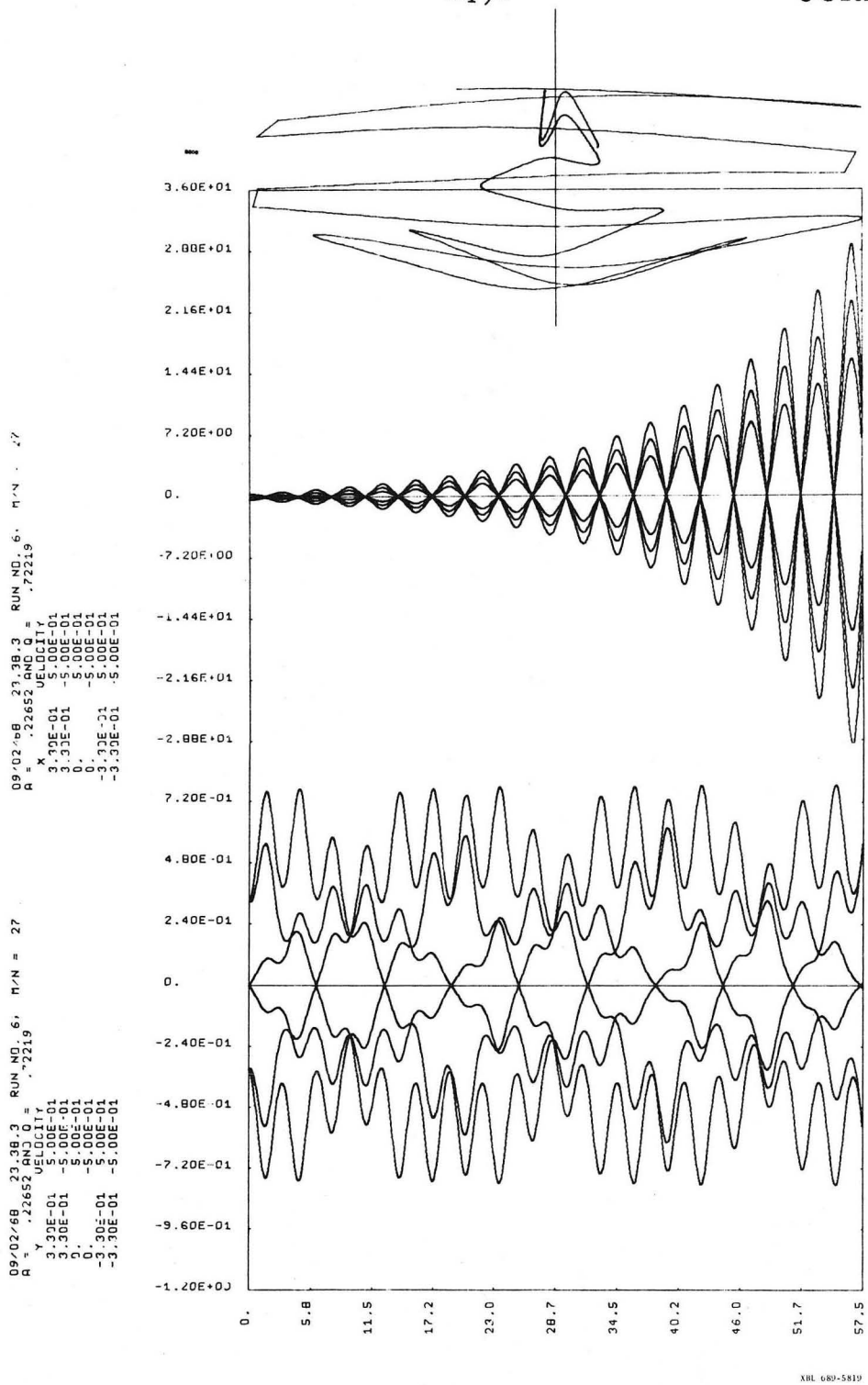

XBL 689-5819

Fig. 15

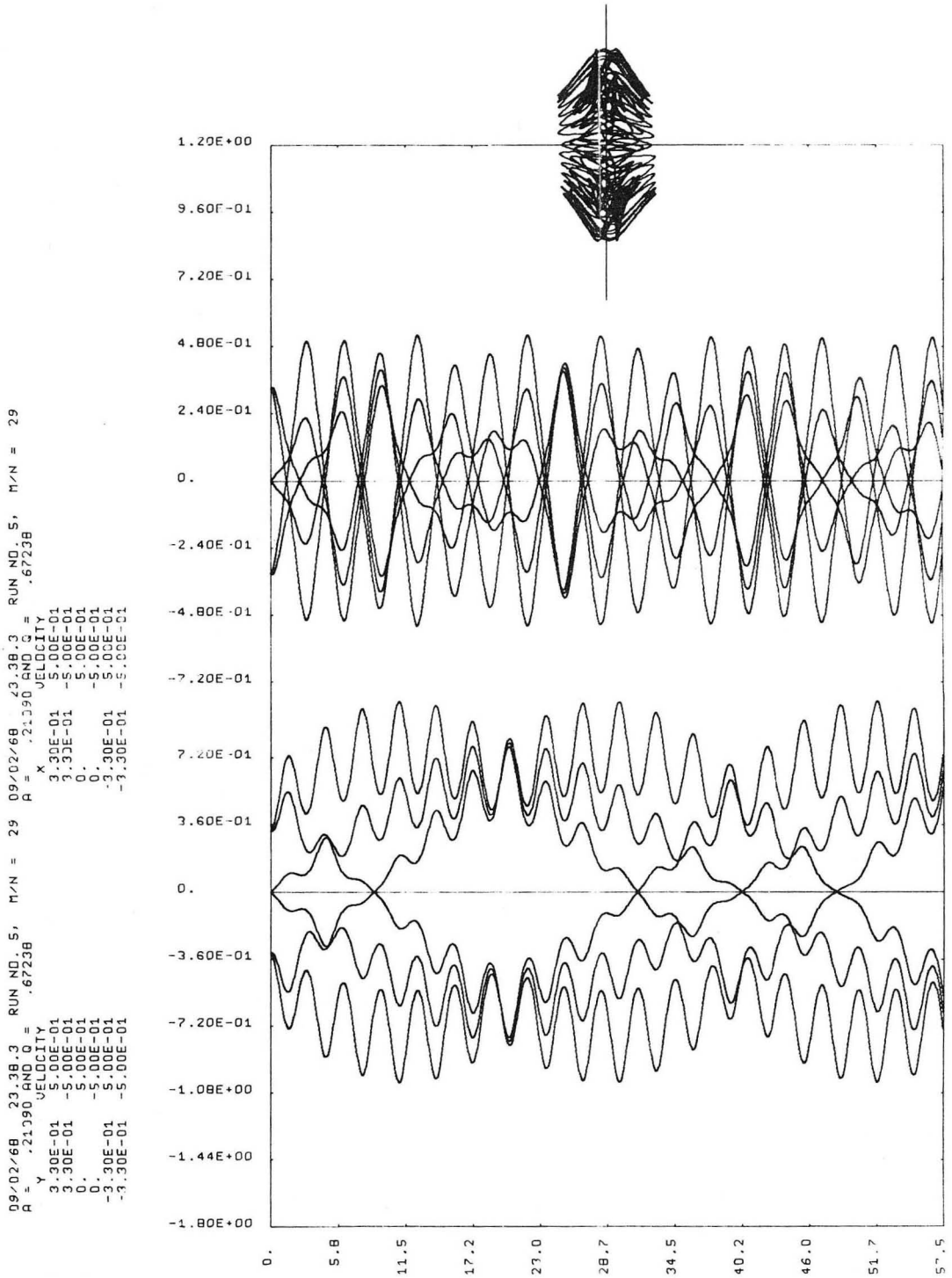

XBL 689-5818

Fig. 16

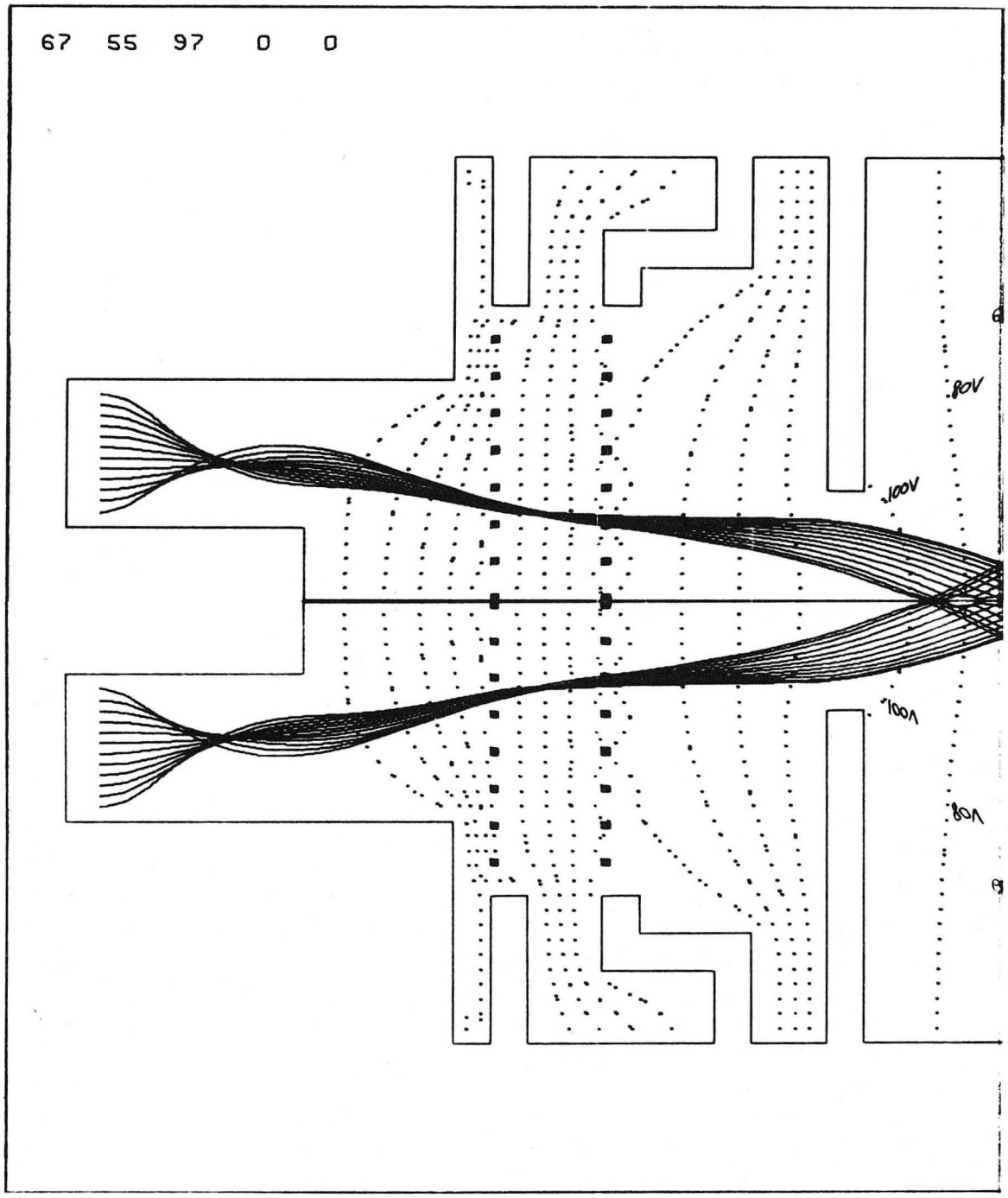

XBL 689-5866

Fig. 17

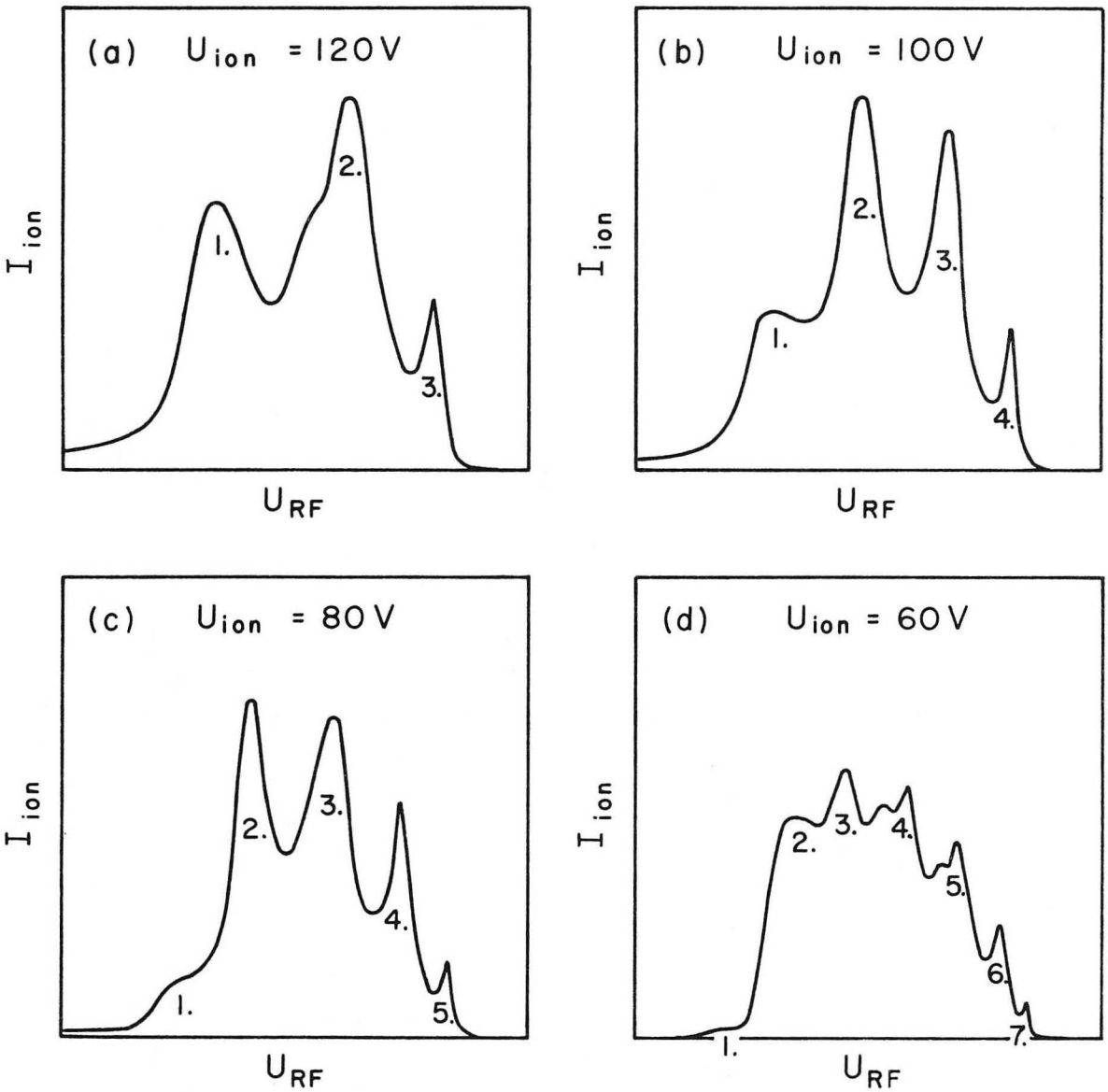

XBL687-3292

Fig. 18

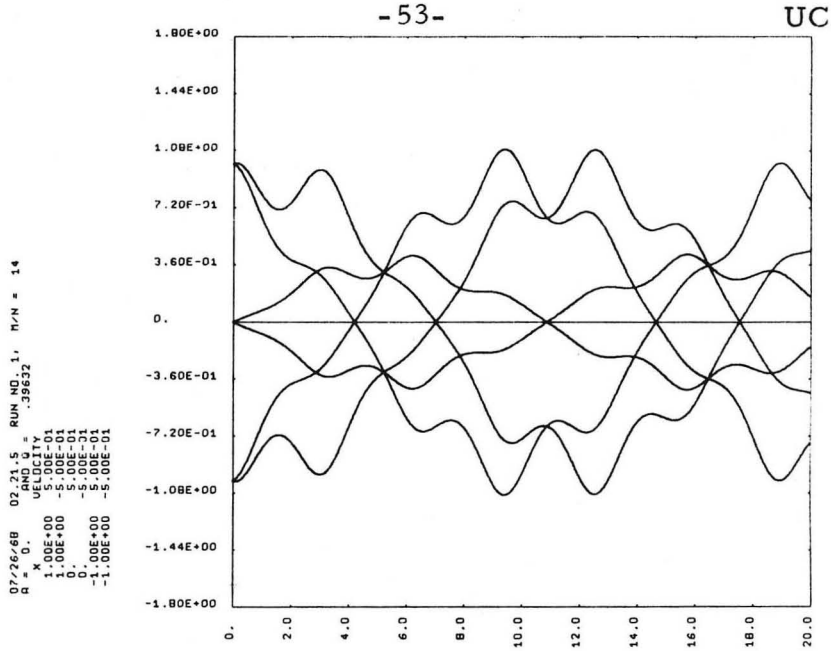

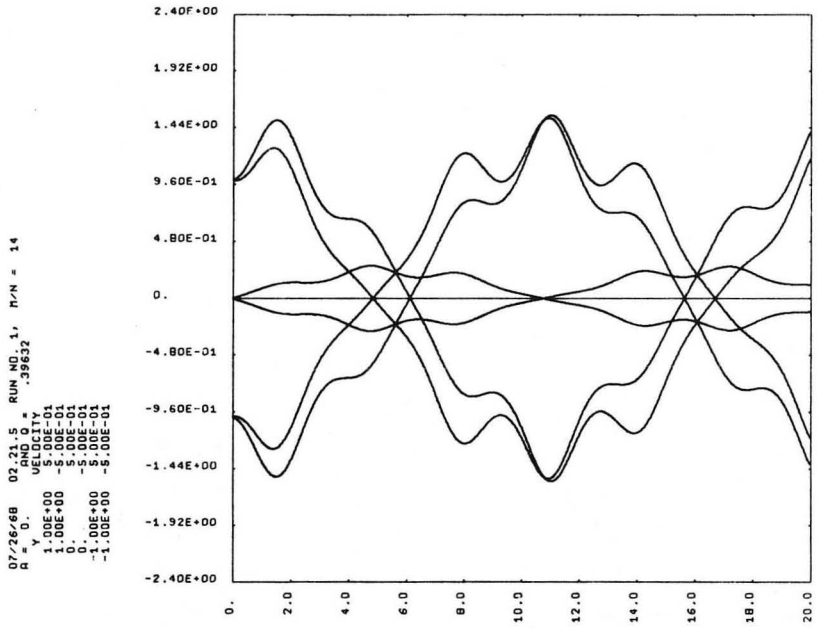

XBL 689-5883

Fig. 19

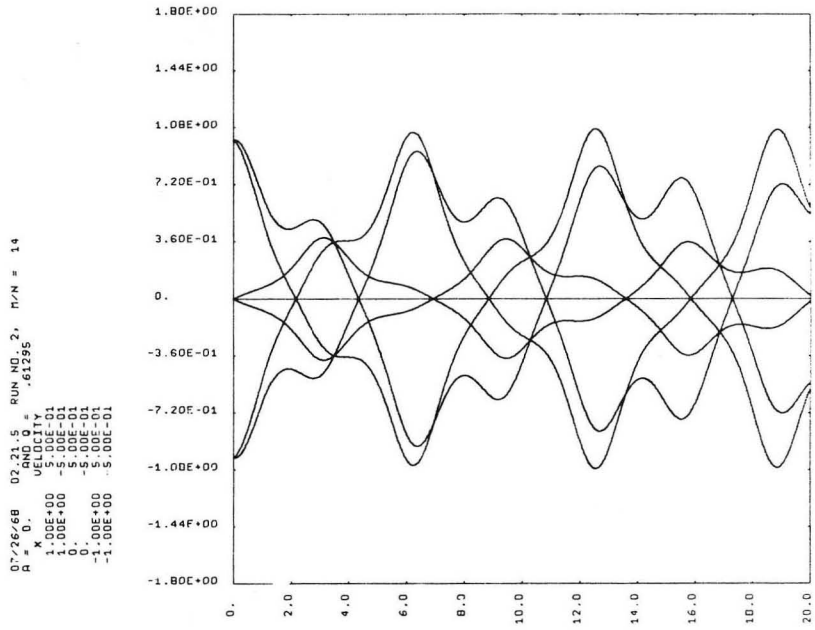

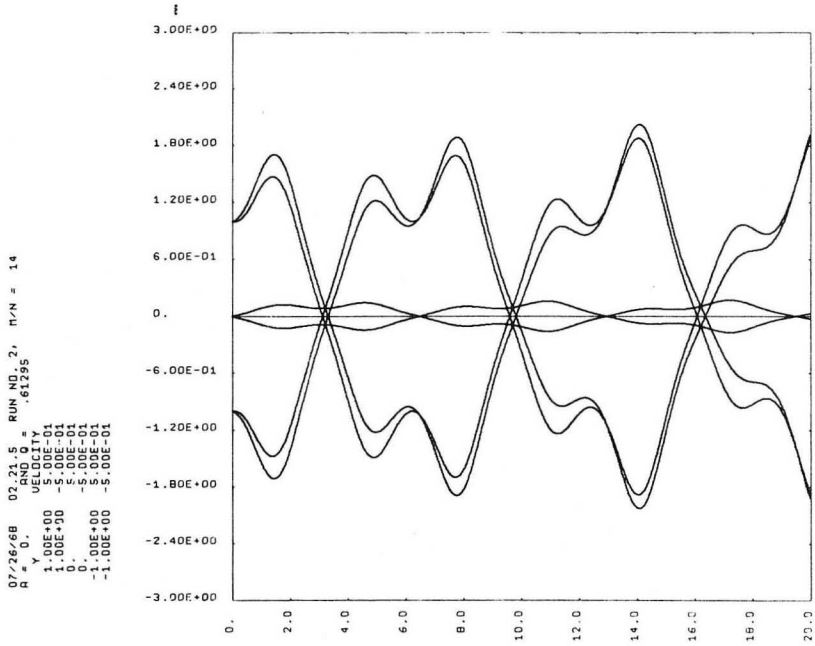

XBL 689-5882

Fig. 20

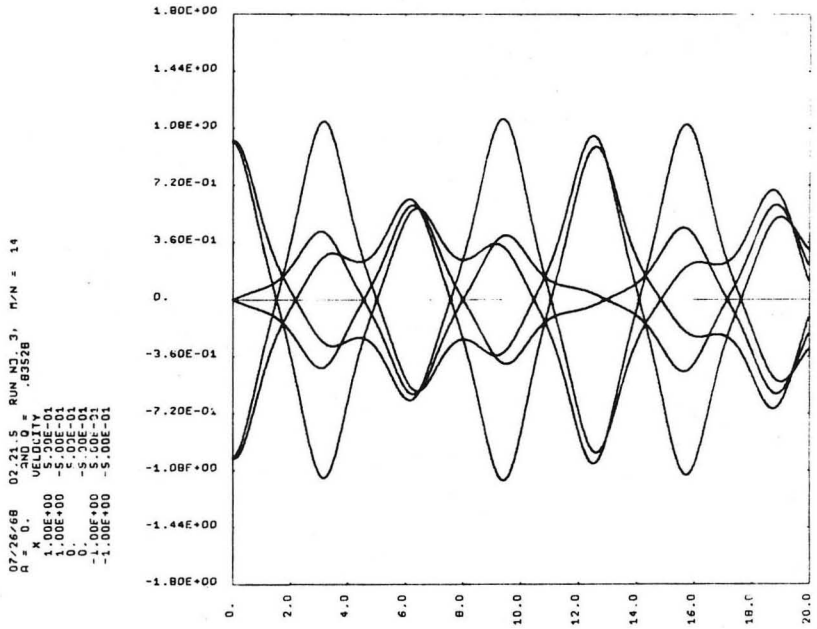

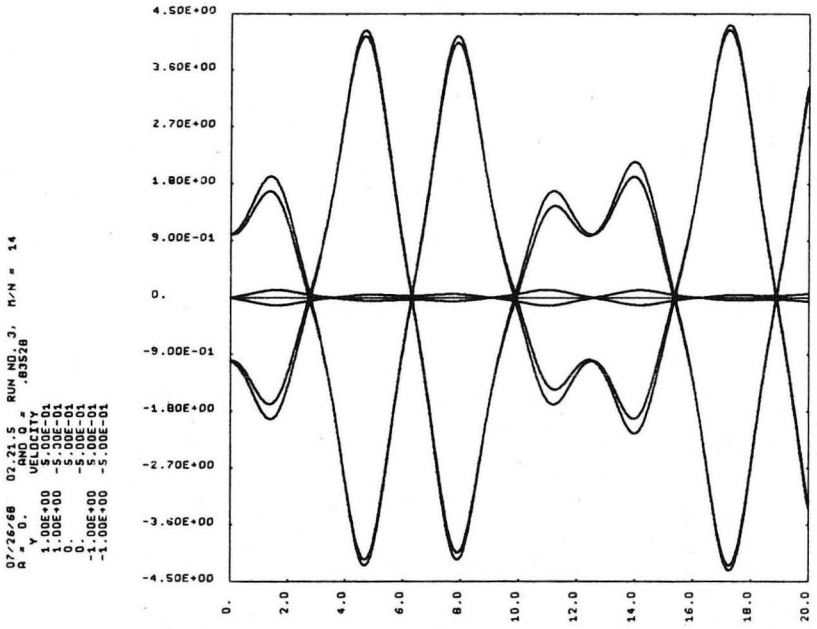

XBL 689-5884

Fig. 21

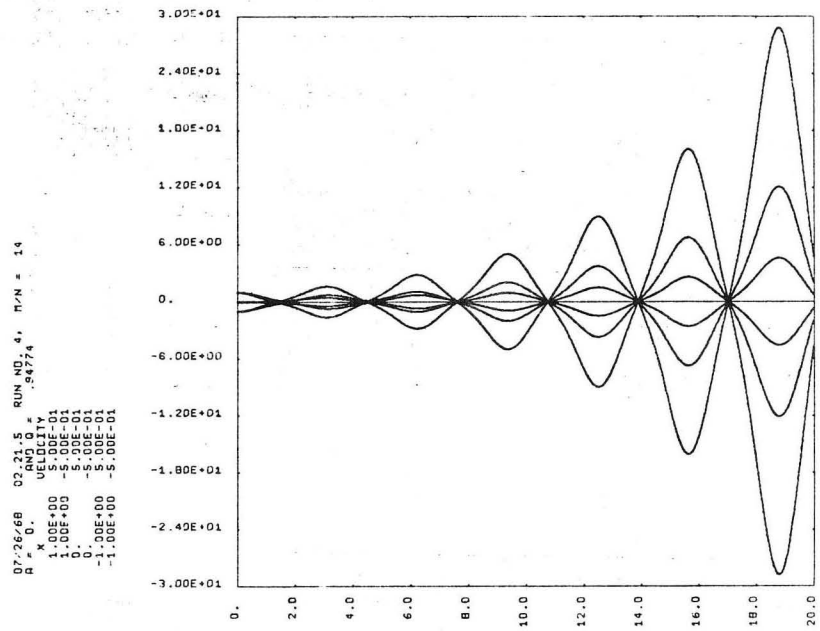

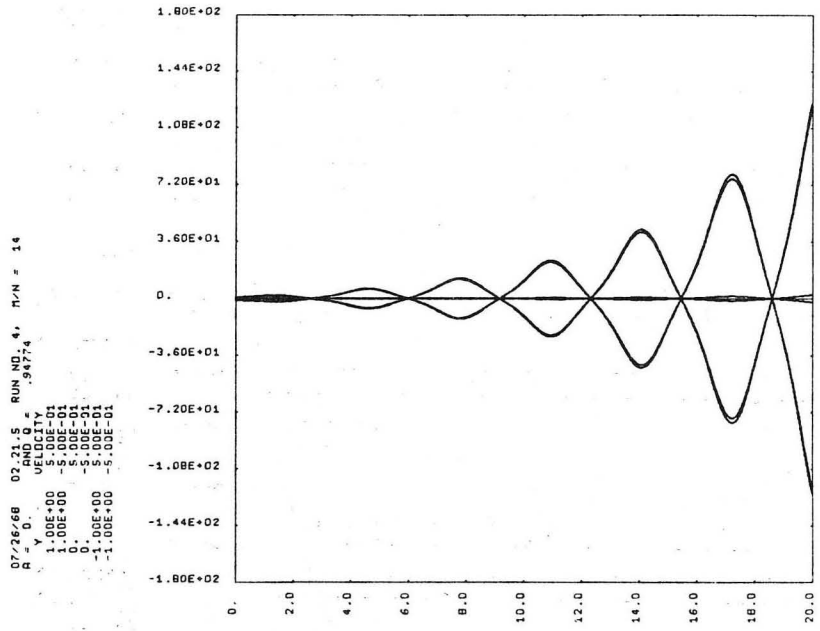

XBL 689-5881

Fig. 22

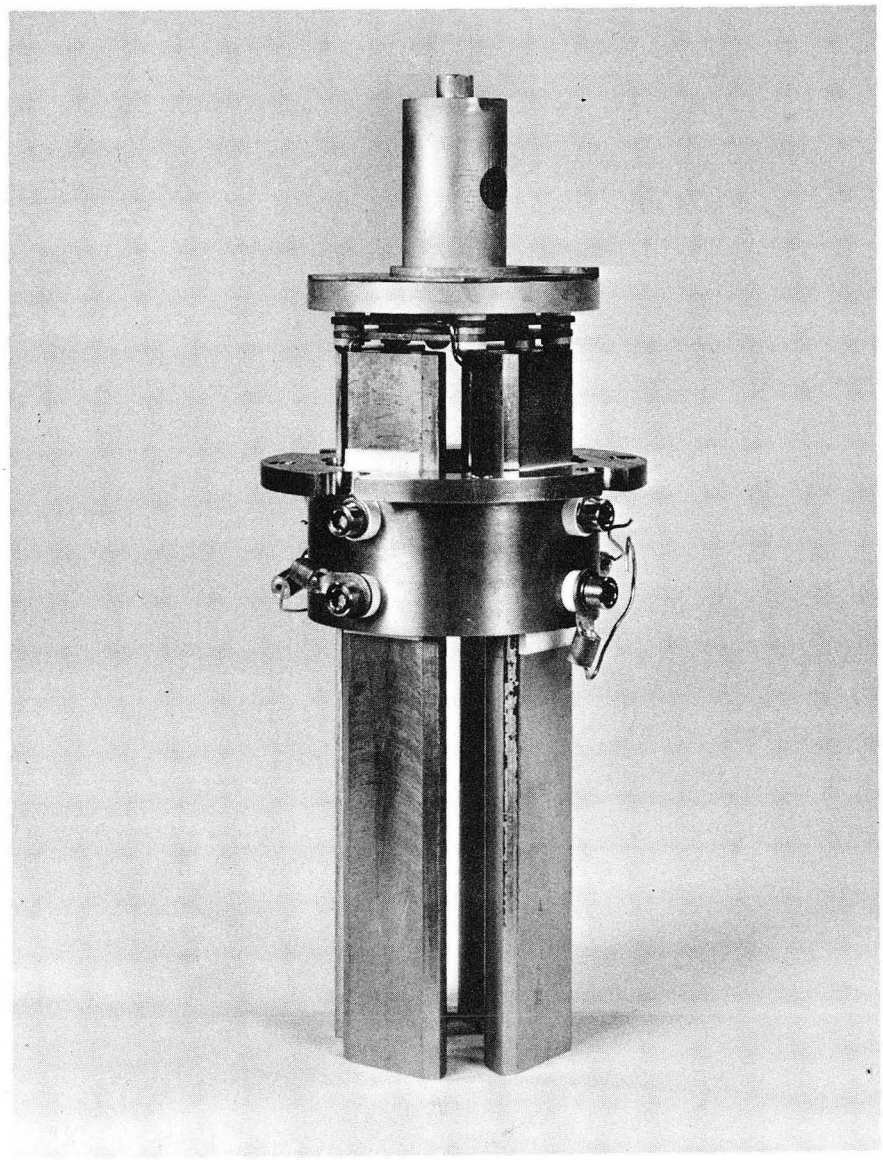

CBB 688-4927

Fig. 23.

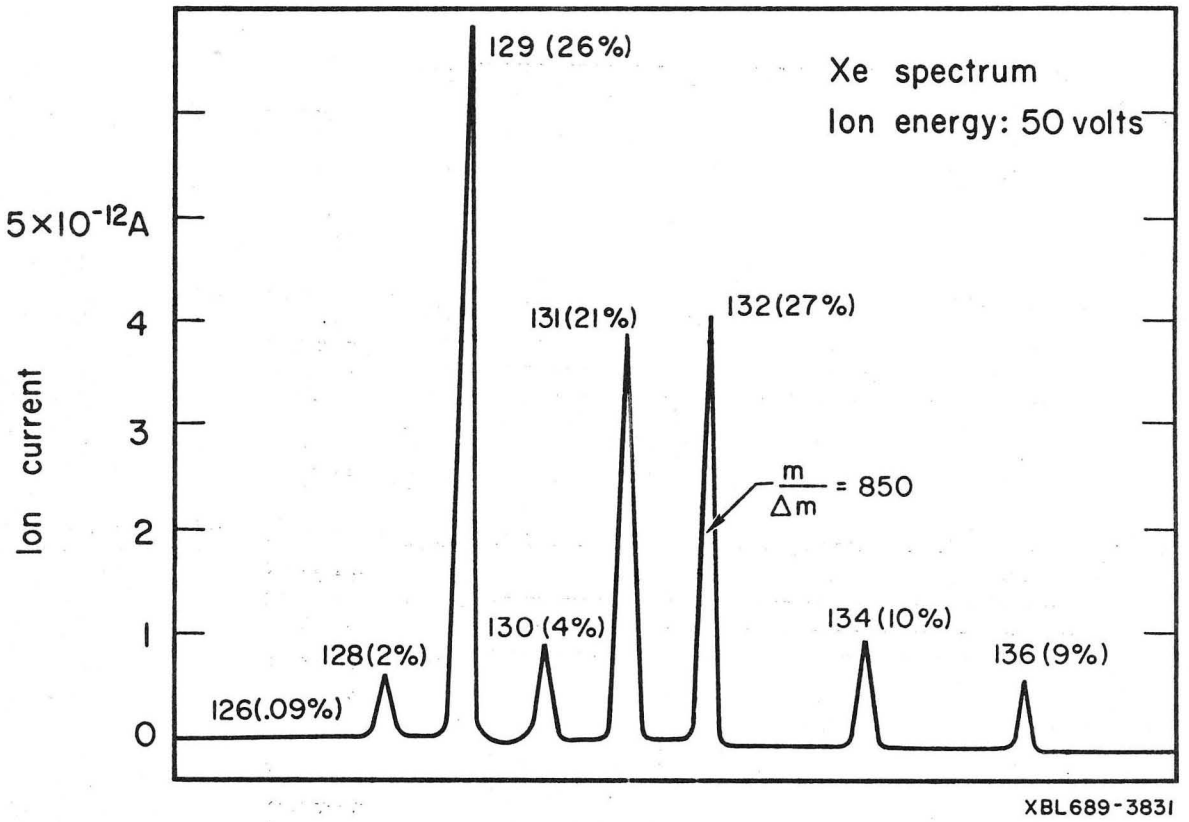
Xe spectrum
Ion energy: 50 volts
129 (26%)
131(21%)
132(27%)
130 (4%)
128(2%)
126(.09%)
134 (10%)
136 (9%)
m/Δm = 850
5×10⁻¹²A
4
3
2
1
0
Ion current
XBL689-3831

Fig. 24

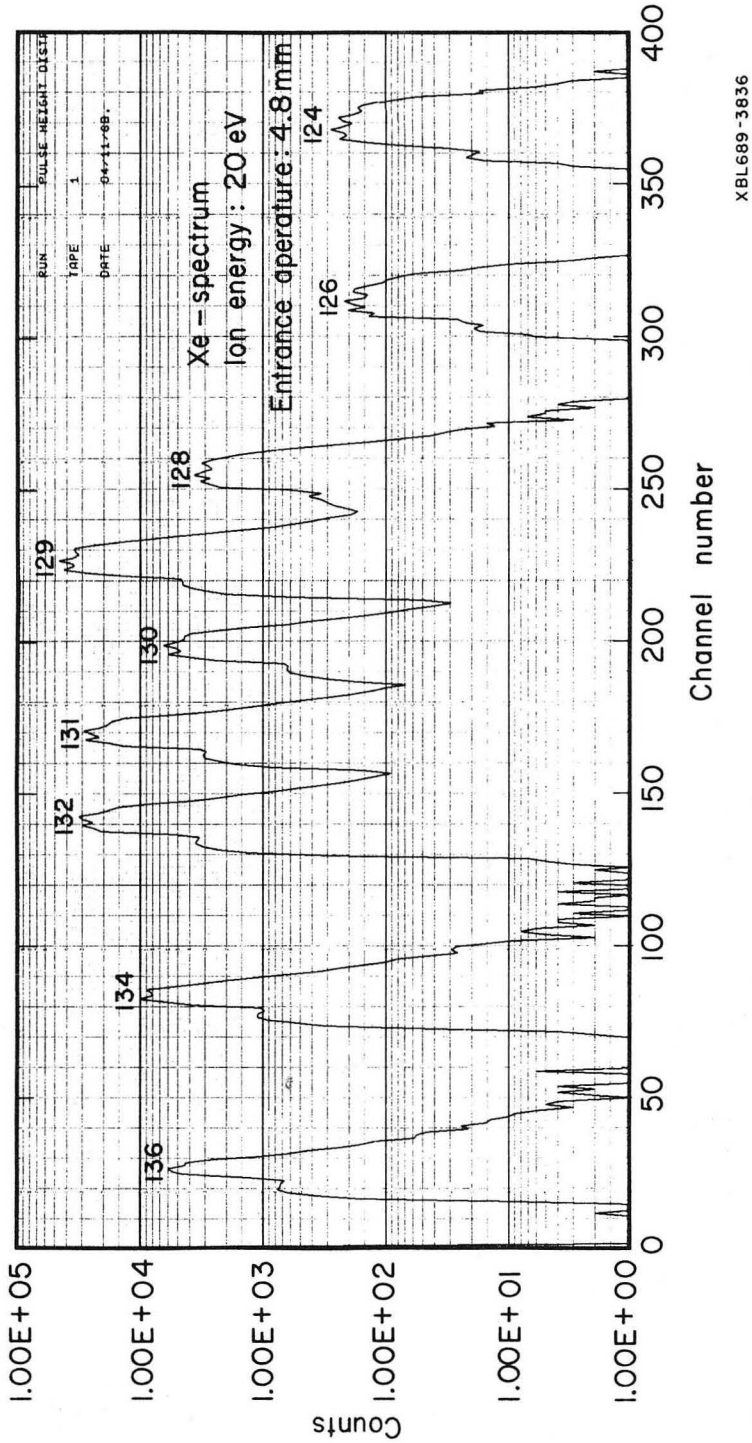
PULSE HEIGHT DISTR
RUN
TAPE 1
DATE 04-11-68.
Xe - spectrum
Ion energy : 20 eV
Entrance aperature : 4.8 mm
124
126
128
129
130
131
132
134
136
Counts
1.00E+05
1.00E+04
1.00E+03
1.00E+02
1.00E+01
1.00E+00
0
50
100
150
200
250
300
350
400
Channel number
XBL689-3836

Fig. 25

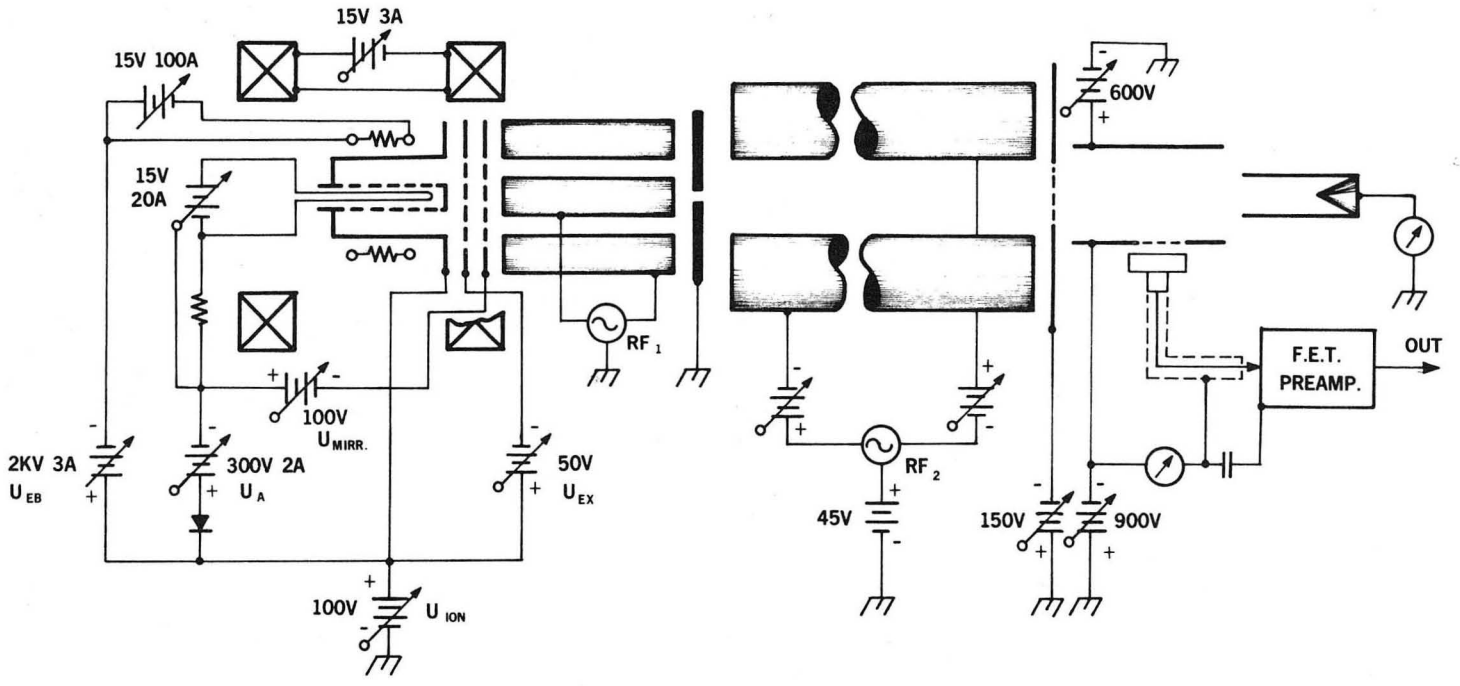
15V 3A
15V 100A
15V
20A
100V
U MIRR.
2KV 3A
U EB
300V 2A
U A
50V
U EX
100V
U ION
RF 1
RF 2
45V
600V
150V
900V
F.E.T.
PREAMP.
OUT

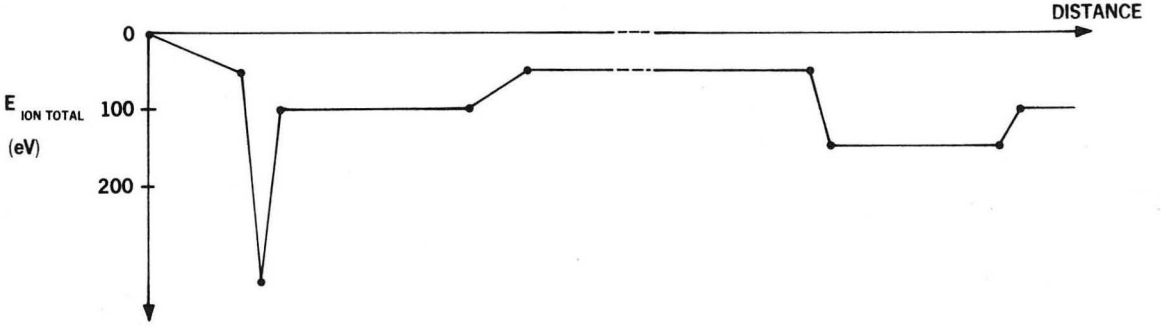
DISTANCE
0
E ION TOTAL
(eV)
100
200

Fig. 26

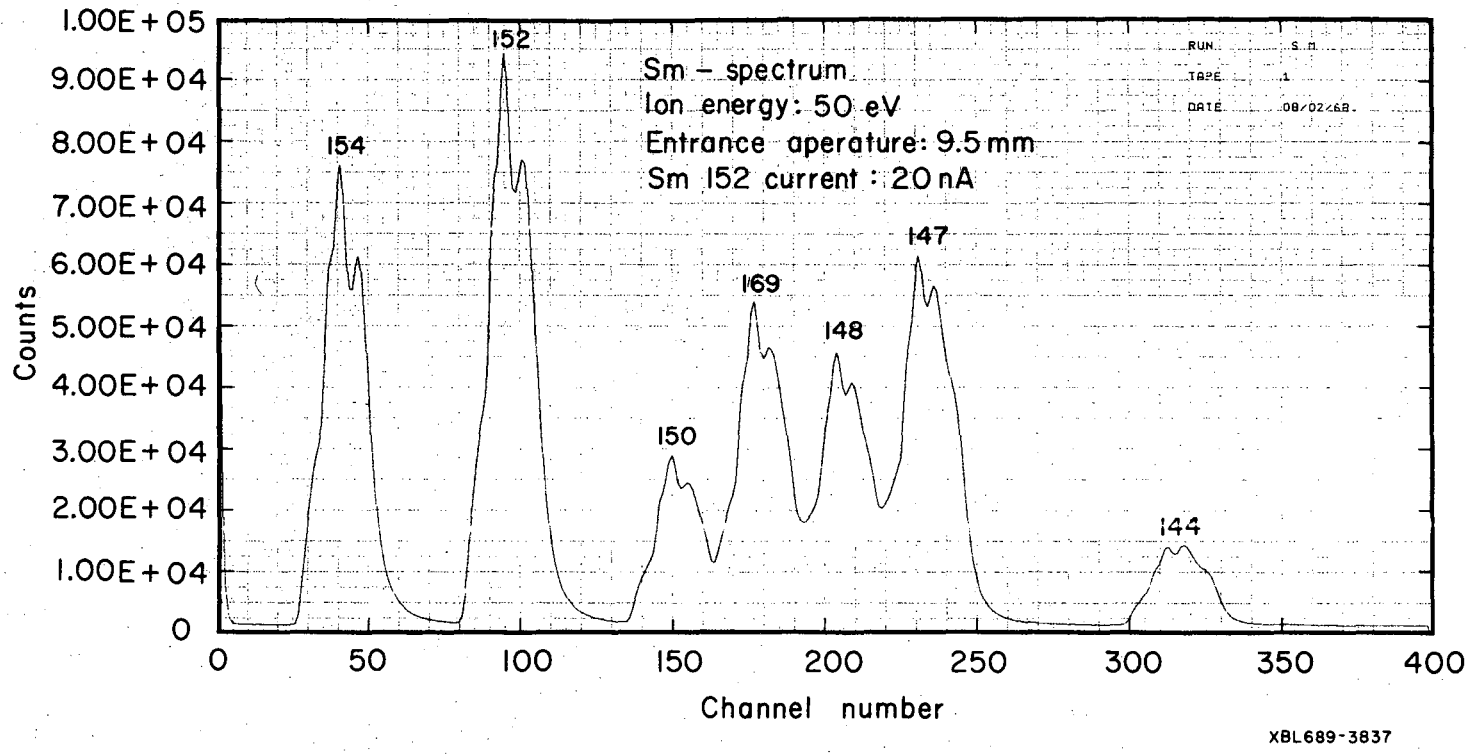
Sm – spectrum
Ion energy: 50 eV
Entrance aperature: 9.5 mm
Sm 152 current : 20 nA
RUN
TAPE
DATE
154
152
150
169
148
147
144
Counts
1.00E+05
9.00E+04
8.00E+04
7.00E+04
6.00E+04
5.00E+04
4.00E+04
3.00E+04
2.00E+04
1.00E+04
0
0
50
100
150
200
250
300
350
400
Channel number
XBL689-3837

Fig. 27

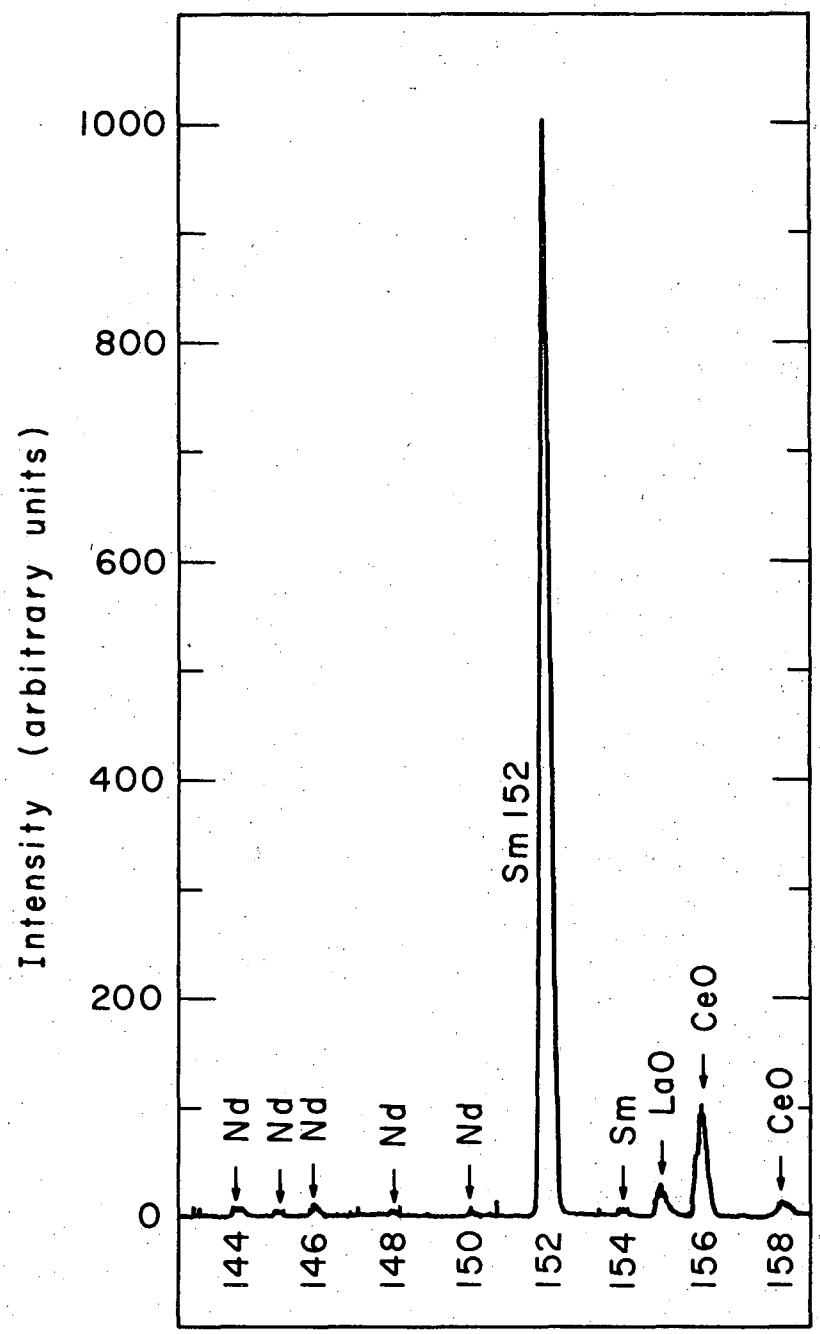

Mass analysis of separated Sm 152

XBL687-3289

Fig. 28

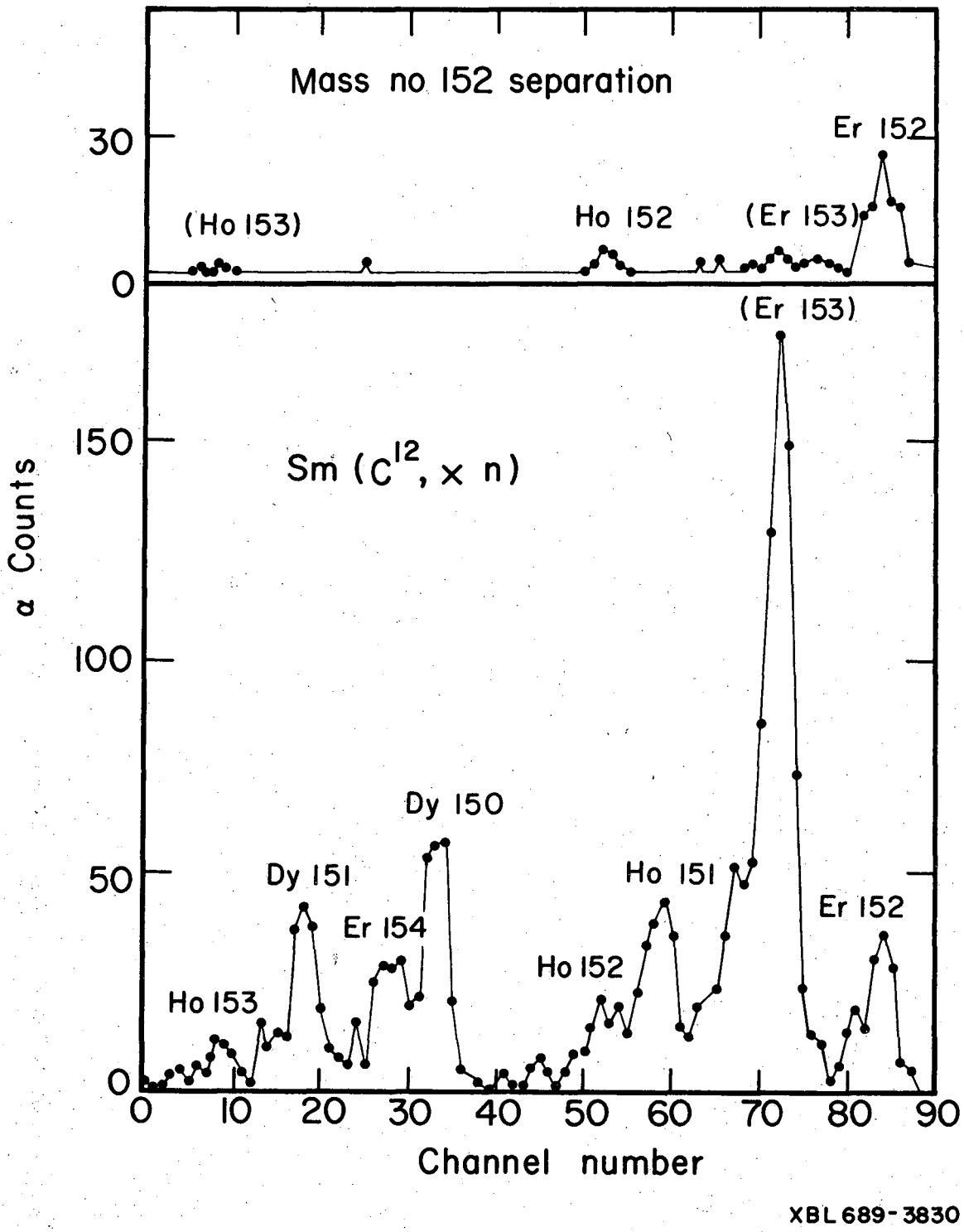
Mass no 152 separation
Er 152
(Ho 153)
Ho 152
(Er 153)
30
0
(Er 153)
150
Sm (C^{12}, x n)
α Counts
100
Dy 150
50
Dy 151
Ho 151
Er 154
Er 152
Ho 152
Ho 153
0
0 10 20 30 40 50 60 70 80 90
Channel number
XBL 689-3830

Fig. 29

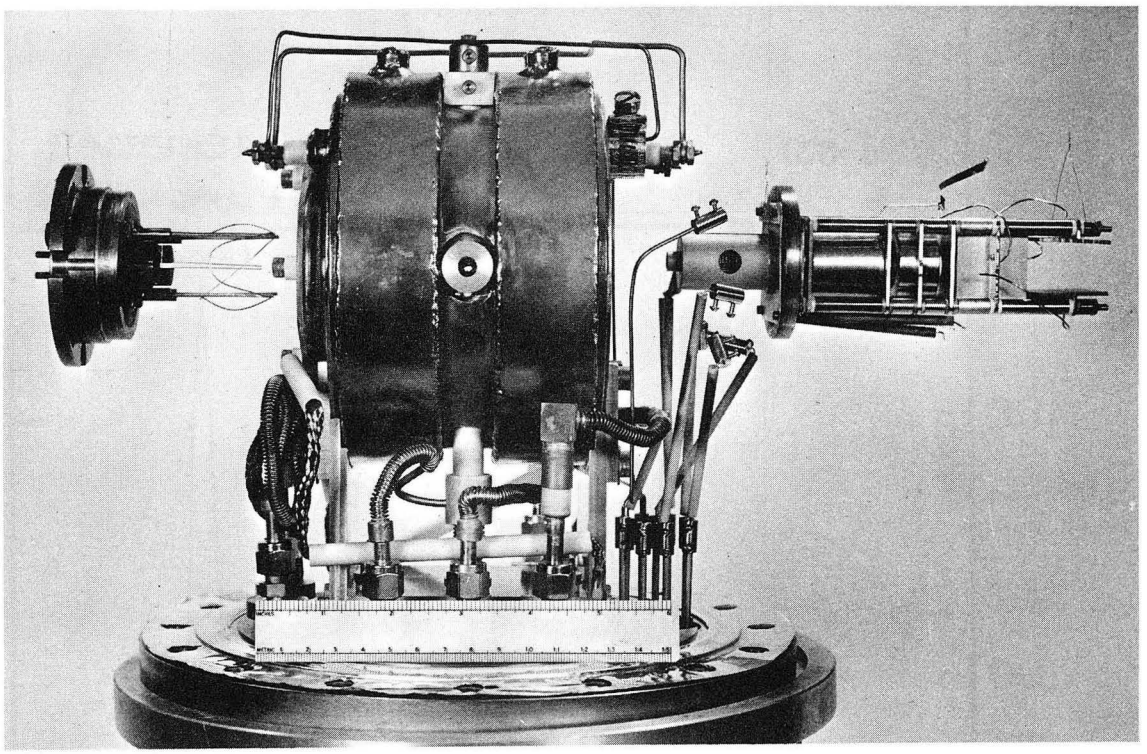

CBB 682-891

Fig. 30.

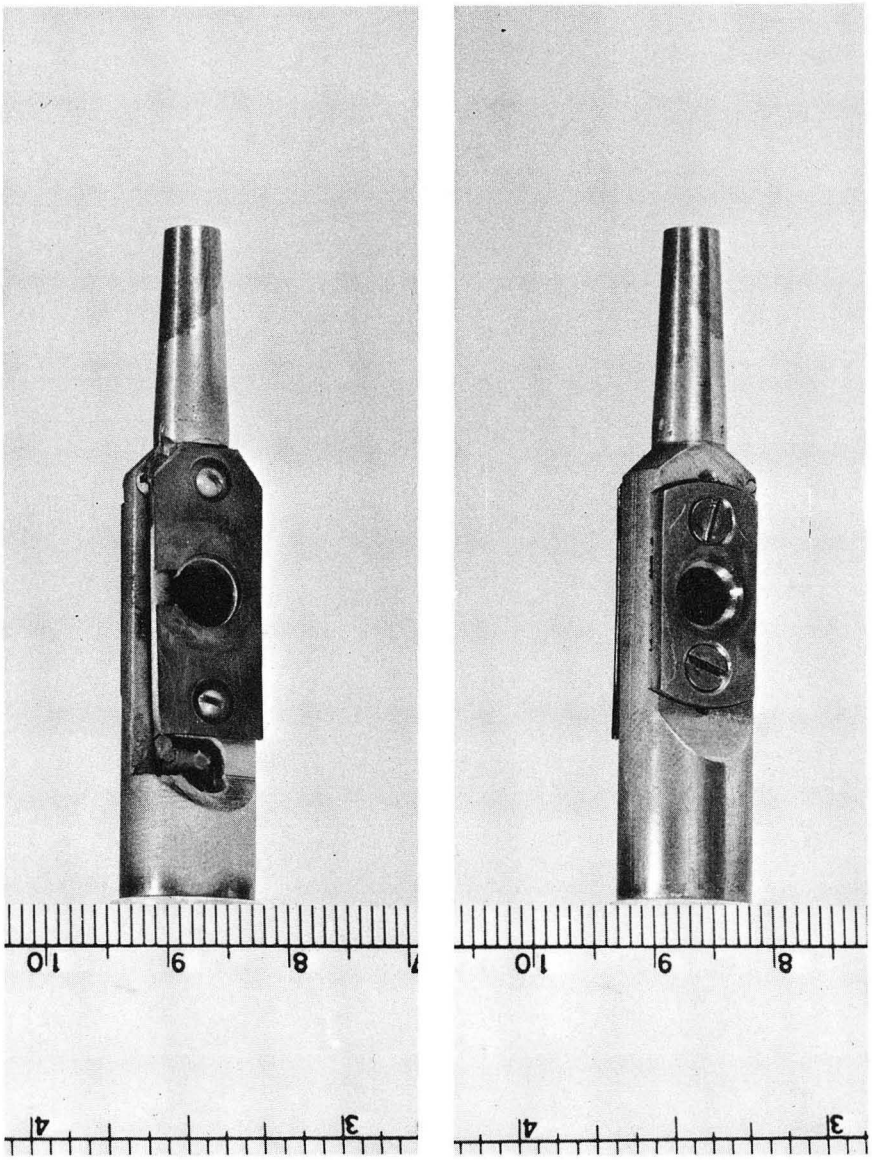

CBB 688-4882

Fig. 31.

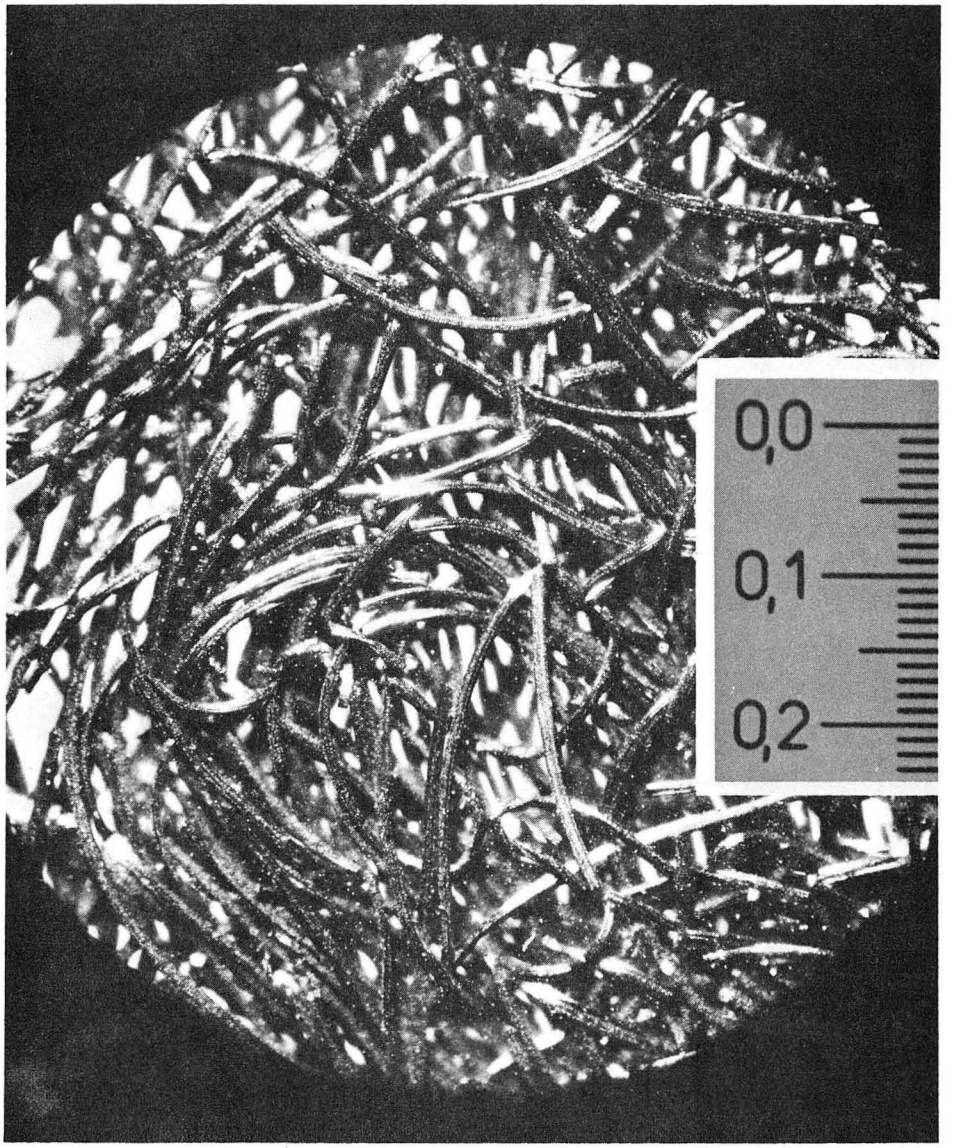

XBB 688-4665

Fig. 32.

This report was prepared as an account of Government sponsored work. Neither the United States, nor the Commission, nor any person acting on behalf of the Commission:

A. Makes any warranty or representation, expressed or implied, with respect to the accuracy, completeness, or usefulness of the information contained in this report, or that the use of any information, apparatus, method, or process disclosed in this report may not infringe privately owned rights; or

B. Assumes any liabilities with respect to the use of, or for damages resulting from the use of any information, apparatus, method, or process disclosed in this report.

As used in the above, "person acting on behalf of the Commission" includes any employee or contractor of the Commission, or employee of such contractor, to the extent that such employee or contractor of the Commission, or employee of such contractor prepares, disseminates, or provides access to, any information pursuant to his employment or contract with the Commission, or his employment with such contractor.